NASA TECHNICAL NOTE

NASA TN D-4746

DRAG DUE TO TWO-DIMENSIONAL SURFACE ROUGHNESS IN A TURBULENT BOUNDARY LAYER AT MACH 3 WITH AND WITHOUT HEAT TRANSFER

by William J. Monta, K. R. Czarnecki, and William D. Deveikis

Langley Research Center
Langley Station, Hampton, Va.

NATIONAL AERONAUTICS AND SPACE ADMINISTRATION • WASHINGTON, D. C. • SEPTEMBER 1968

NASA TN D-4746

DRAG DUE TO TWO-DIMENSIONAL SURFACE ROUGHNESS IN A TURBULENT BOUNDARY LAYER AT MACH 3 WITH AND WITHOUT HEAT TRANSFER

By William J. Monta, K. R. Czarnecki, and William D. Deveikis

Langley Research Center
Langley Station, Hampton, Va.

NATIONAL AERONAUTICS AND SPACE ADMINISTRATION

For sale by the Clearinghouse for Federal Scientific and Technical Information
Springfield, Virginia 22151 – CFSTI price $3.00

DRAG DUE TO TWO-DIMENSIONAL SURFACE ROUGHNESS IN A TURBULENT BOUNDARY LAYER AT MACH 3 WITH AND WITHOUT HEAT TRANSFER

By William J. Monta, K. R. Czarnecki,
and William D. Deveikis
Langley Research Center

SUMMARY

An investigation has been conducted at Mach 3 on an ogive-cylinder model to determine the effect of heat transfer on the drag due to two fabrication roughness shapes (steps with grooves and circular arc waves) at Reynolds numbers from 36×10^6 to 195×10^6. The results indicate only a slight effect of heat transfer and Reynolds number upon the roughness drag for the two configurations of the investigation. The zero heat-transfer data are in good agreement with previously published results. The step roughness drag is correlated on the basis of a step-height Reynolds number and is in good agreement with both existing data and an existing prediction method based on "effective dynamic pressure." For the wave-shaped wall, a nondimensional drag parameter was found to be a function of the ratio of roughness height to boundary-layer thickness h/δ for a constant value of the roughness thickness ratio h/l. At the lower values of h/l, the parameter is a unique function of the ratio of roughness cycle length to boundary-layer thickness l/δ.

INTRODUCTION

The increased importance of the drag of fabrication-type surface roughness to the performance of the more efficient supersonic airplane configurations has led to a number of experimental investigations which were reported in references 1 to 4. These investigations were conducted at zero heat transfer for a range of test conditions and have indicated that the drag of roughness would largely be related to the local conditions in the boundary-layer flow. Because changes in Reynolds number and in heat transfer contribute to large changes in the boundary-layer velocity profiles near the wall, it might be expected that they would also have a large effect upon the drag of roughness elements.

The present investigation was conducted in order to study the effect of heat transfer and high Reynolds number on the drag of two sample roughness shapes. Some of the preliminary results were presented in reference 5. Force and pressure measurements

were made on three 3.1-meter-long ogive cylinder models having different surface conditions on their cylindrical sections (that is, smooth, steps with grooves, and circular-arc waves). The tests were made with a turbulent boundary layer at a Mach number of 3 over a range of unit Reynolds numbers from 12×10^6 to 63×10^6 per meter, and for ratios of model-wall temperature to free-stream temperature from 1.4 to 2.6.

SYMBOLS

$C_{D,b}$ base pressure drag coefficient, $\frac{p_\infty - p_b}{q_\infty} \frac{S_{base}}{S_{ref}}$

$C_{D,p}$ nose pressure drag coefficient, $\int_0^1 C_p d\left(\frac{r}{R}\right)^2$

$C_{D,R}$ roughness drag coefficient, $\Delta C_{D,s} \frac{S_w}{S_f} \frac{q_\infty}{q_\delta}$ or $\frac{\text{Drag increment due to roughness}}{S_f q_\delta}$

$C_{D,s}$ free-stream coefficient of surface drag (skin friction plus roughness pressure drag), $\left(C_{D,T} - C_{D,p} - C_{D,b}\right) \frac{S_{ref}}{S_w}$

$\Delta C_{D,s}$ increment in drag coefficient, $C_{D,s} - \left(C_{D,s}\right)_{smooth}$

$C_{D,T}$ total drag coefficient, $\frac{D}{q_\infty S_{ref}}$

C_F average skin-friction drag coefficient for smooth body, $\left(C_{D,s}\right)_{smooth}$

C_p pressure coefficient, $\frac{p - p_\infty}{q_\infty}$

D total drag measured by balance

h roughness-element height

L length of complete model

l roughness-element cycle length

M Mach number

p pressure

p'	measured pitot pressure
q	dynamic pressure, $0.7pM^2$
R	radius of cylinder
R_h, R_L, R_x	free-stream Reynolds number based upon h, L, and x, respectively
r	local body radius
r_{max}	body radius at top of roughness
r_{min}	body radius at bottom of roughness
S	area
S_f	total frontal area of roughness, $\pi\left(r_{max}^2 - r_{min}^2\right)$ (number of roughness cycles)
S_{ref}	reference area, πR^2
T	temperature
T'	reference temperature (eq. (4))
t	time
x	axial distance to center of a series of roughness elements
$\beta = \sqrt{M_\infty^2 - 1}$	
δ	total boundary-layer thickness
θ	momentum thickness
η_r	temperature recovery factor, $\frac{T_{aw} - T_\infty}{T_{t,\infty} - T_\infty}$
ϕ	azimuth angle measured clockwise from top dead center of model when viewed from rear

Subscripts:

b	conditions at base of model
rough	model with roughness elements
smooth	smooth model
t	stagnation conditions
w	wetted area, or wall
∞	free stream
δ	conditions outside boundary layer
av	average
aw	adiabatic

Superscript:

*	transformed quantity (eqs. (1) and (2))

APPARATUS AND METHODS

Wind Tunnel

The present investigation was conducted in the Langley 9- by 6-foot thermal structures tunnel, a Mach number 3 intermittent blowdown facility exhausting to the atmosphere. This facility operates at stagnation pressures between 379 kN/m^2 and 1379 kN/m^2 and at stagnation temperatures from 422° K to 622° K when preheating is done by using only the metallic-mass heat exchanger. These conditions provide a free-stream unit Reynolds number range from approximately 12×10^6 to 63×10^6 per meter. Data obtained from a limited number of Mach number calibration tests conducted as part of this investigation indicated a random variation of Mach number with tunnel stagnation pressure and stagnation temperature. The average test-section Mach number was determined to be 2.977 ± 0.015. Results from these tests are discussed in the appendix. A more detailed description of the test facility can be found in reference 6.

Models

Three models were tested in this investigation. The reference configuration was a smooth 3.1-meter-long, 25.4-cm-diameter, 3-caliber-nose, ogive cylinder as shown in figure 1. The cylindrical sections of the second and third models had different two-dimensional fabrication-type surfaces (fig. 1(b)). One was constructed with 24 protruding waves consisting of constant-chord, circular-arc profiles, and the other had 11 alternating forward- and rearward-facing steps with grooves. All three sets of cylinders were tested in combination with the same smooth ogive nose. A base block, used to minimize the base pressure drag on the model, is shown in the typical position 0.5 cm behind the model. (See fig. 1.) A photograph of the rough cylinders is shown in figure 2. The model nose and cylindrical sections were constructed from stainless steel and had a wall thickness of 0.476 cm. Exterior surfaces were finished to approximately 0.1μ to 0.2μ. As shown in figure 2, the model cylindrical afterbodies were constructed in two pieces. This was done for ease of assembly in the tunnel test section. The model sections were fastened with flat-head screws which were countersunk below the exterior surface. Holes formed by the depressed screw heads were filled flush with the exterior surface by means of a potting compound.

Instrumentation

The models were instrumented to measure: aerodynamic forces and moments, nose pressures, base pressures, skin temperatures, and interior static pressures and temperatures. Forces and moments were measured with a six-component water-cooled strain-gage balance. The provision for cooling was made to maintain a uniform balance temperature and thus to avoid shifts in readings caused by balance temperature changes resulting from heating of the model skin. Static pressures were measured at the 19 locations listed in table I. Four orifices were equally spaced circumferentially at a station 28 centimeters from the nose tip, and the remaining orifices were placed along one meridian. The base plug was instrumented with four equally spaced static-pressure orifices on the face adjacent to the model interior. Fourteen no. 24-gage iron-constantan thermocouples were located along the model length. (See table II.) Eleven were spot-welded to the interior surface and three were installed to read temperatures at the exterior surface. The balance temperature was monitored at four different locations. A high-speed digital magnetic tape system was used to record output from pressure transducers, thermocouples, and force-balance gages.

Tests

The skin-friction models were sting mounted at an angle of incidence of 0° with respect to the tunnel center line. A turbulent boundary layer was maintained by a trip

located 1.6 centimeters from the tip of the model. The trip consisted of 12 pieces of wire 0.025 centimeter in diameter and 0.3 centimeter long spotwelded to the model nose parallel to the model axis. The test program is summarized in table III. Each model was tested over a free-stream unit Reynolds number range from 12×10^6 to 63×10^6 per meter. This range was obtained by testing at stagnation pressures of 414, 690, 1034, and 1380 kN/m^2 and at stagnation temperatures of 422° K and 588° K. In general, the procedure was to begin a run at the 414 kN/m^2 level and proceed in ascending steps to 1380 kN/m^2. In one run (test 4), however, the model was tested only at the 1380 kN/m^2 pressure level. The variation of stagnation pressure and stagnation temperature with time from a typical run is shown in figure 3. The peaks in the stagnation-temperature curve reflect an adiabatic-compression process which occurs when the stagnation pressure is suddenly increased. The period of time at each stagnation-pressure level was selected to permit model pressure gages to reach equilibrium.

The models were tested under heat-transfer conditions and also under essentially zero heat-transfer conditions. The heat-transfer tests were performed by starting the tunnel with the model at room temperature, which is below the recovery temperature for the test conditions. The zero-heat-transfer tests were conducted by preheating the model approximately to the adiabatic wall temperature. This heating was done by circulating hot air over the model which was encased within frangible ducting. Hot air was pumped through the ducting by means of an electrically powered air heater. With this system, the temperature variation from model nose to base could be held within 28° K. Upon reaching the desired model temperature, the tunnel was started and the ducting was destroyed and removed by the airstream. Model damage from ducting fragments was negligible.

Reduction of Data

Experimental skin-friction coefficients were determined by subtracting base-pressure and nose-pressure drags from the total drag as measured by the balance so that

$$C_{D,s} = \left(C_{D,T} - C_{D,p} - C_{D,b}\right)\frac{S_{ref}}{S_w}$$

All test data were averaged arithmetically over 10 consecutive data frames which are equivalent to 0.50 second of data for the normal sampling rate of 20 frames per second. This averaging was done to "damp out" the higher frequency balance output fluctuations not damped electrically by the test recording system.

Skin-friction results were transformed to the incompressible-form values $C_F{}^*$ and $R_L{}^*$ by means of the Sommer and Short T' method (ref. 7) so that

$$C_F^* = \frac{C_F}{T'/T_\infty} \tag{1}$$

$$R_L^* = R_L\left(\frac{R_{L,T'}}{R_{L,\infty}}\right) \tag{2}$$

where

$$\frac{T'}{T_\infty} = 1 + 0.0035M^2 + 0.45\left(\frac{T_{w,av}}{T_\infty} - 1\right) \tag{3}$$

and

$$\frac{R_{L,T'}}{R_{L,\infty}} = \left(\frac{T_\infty}{T'}\right)^{5/2}\left(\frac{T' + 198.6}{T_\infty + 198.6}\right) \tag{4}$$

The quantity $T_{w,av}$ is a weighted average of the individual model wall temperatures. The weighting system assigns to each thermocouple an area equal to one-half of the model surface area between it and the adjacent thermocouples.

RESULTS AND DISCUSSION

Typical Model Temperatures

Some sample model temperatures are presented for a heat-transfer run in figure 4(a) and a zero-heat-transfer run in figure 4(b). It can be seen that the midsection of the model, which could not be instrumented with thermocouples, lies in a region of approximately constant wall temperatures. The weighted average temperatures, indicated by solid symbols, are seen to be only slightly higher than the local temperature on the cylindrical portion of the model. Not indicated are data from three thermocouples A, B, and C which resulted in outside wall temperatures from 0° K to 2° K higher than the inside wall values presented.

The temperature distributions for the zero-heat-transfer conditions (model preheated) of figure 4(b) are more uniform than those for the case of heat transfer (fig. 4(a)). The estimated T_{aw} is shown for comparison on the basis that $\eta_r = 0.89$, T_t is evaluated at free-stream conditions, and local Mach number is predicted by the theory of characteristics. The 25° C experimental temperature variation from the nose to the base of the model is the result of the present preheating process and is changed only slightly during the test as a result of aerodynamic heat transfer.

Nose Pressure Distribution

The results of the ogive nose pressure measurements at $p_{t,\infty} = 1380$ kN/m^2 are shown in figure 5. Data of figure 5(a) are measured along a single model ray. The

correlation curve based on characteristics theory was used as a guide to fairing. The repeatability of data from different runs is generally very good. In addition, a small amount of data (not shown) which were measured at $p_{t,\infty} = 690$ and 1034 kN/m^2 fell within a C_p of ± 0.002 of the 1380 kN/m^2 points. Evaluation of the faired curve of the experimental data yielded a nose pressure drag coefficient of 0.9037.

The variation in measured pressure coefficient with an azimuth angle for four 90^o positions around the model nose at the $x = 28.04$ centimeters station is shown in figure 5(b) for three test runs. The maximum variation in C_p around this station is approximately 0.0025 from the mean. This result indicates some combination of slight model nose misalinement with the free stream and geometrical imperfection of the nose profile.

Smooth-Body Skin Friction

Sample variation with time.- The computer results of a typical run for the smooth body are presented in figure 6 where $T_{w,av}/T_\infty$, R_L, and C_F are plotted against time. These results are from the same run as was used in figure 3. As a result of the continuous increase of average model wall temperature ratio $T_{w,av}/T_\infty$ with time (due to transient heating of the model), the skin-friction coefficient exhibits a corresponding decrease with time.

Steady-state data.- In order to account for the combined variation of temperature and skin friction conveniently, the smooth-body skin friction is shown in terms of transformed coefficients in figure 7. The quantities are transformed to the incompressible form through the use of the Sommer and Short T' skin-friction method (eqs. (1) and (2)). All three heat-transfer conditions are presented: preheated model $(T_w \approx T_{aw})$ at $T_{t,\infty} = 422^o$ K, and the $T_{t,\infty} = 422^o$ K and 588^o K conditions where the runs were started with the model initially at room temperature. All the data tend to group together in good agreement, and fall approximately 12 percent below the reference flat-plate Karman-Schoenherr curve except at the lowest Reynolds number. The duplicate conditions of the tests indicate repeatability within ± 0.00005 (or ± 4 percent) for C_F at the highest Reynolds number. This value represents reasonably good repeatability when the nature of the experimental process involved is considered. The good agreement among the data at various heat-transfer conditions indicates the adequacy of the Sommer and Short method for predicting the effect of heat transfer on skin friction at $M = 3.0$ for the range of $T_{w,av}/T_\infty$ and R_L of these tests. (See ref. 8.) The data would be expected to be somewhat higher than the flat-plate theory predictions because of the three-dimensional boundary-layer-flow effects. Inasmuch as the level of flat-plate theory has been fairly well documented through the lower Reynolds numbers encountered in these tests, it is believed that the absolute level of the present data is probably incorrect. The

uncertainty that exists in the reference smooth-body skin friction is probably due to nose pressures or other sources that would not seriously affect the incremental drag values which are presented in this report.

Drag Due to Roughness

Effect of heat transfer.- The results for the two roughness configurations are presented individually by Reynolds number in figure 8. The variation of drag coefficient with wall-temperature ratios is shown for several Reynolds numbers. The smooth model data are shown for reference purposes. The roughness results appear to be higher than the smooth-body value by constant amounts, but this difference can be seen more clearly in figure 9.

In figure 9 the increment in drag between the smooth and rough bodies $\Delta C_{D,s}$ is shown for all Reynolds numbers. There is only a small change in drag increment with change in wall-temperature ratio, and the greatest variation, which amounts to about 6 percent, occurs for the wave. It is apparent that there is very little effect of heat transfer on the drag due to two-dimensional roughness for the present range of test conditions.

It would be expected that heat transfer could have a substantial effect on the drag of a step roughness at some step height although no effect was seen for the present investigation. The greatest effect might reasonably occur when the step has a height equal to the height of the portion of the boundary-layer flow having the greatest change in dynamic pressure due to heat transfer. Sample calculations indicate that heat transfer causes a progressively greater percentage increase in dynamic pressure with decrease in distance to the wall. Application of the step-drag-prediction method of reference 9 to the heat-transfer case indicates that reducing step height from the 0.109-centimeter value of the present investigation increases the effect of heat transfer. At one-eighth of the present step height the drag coefficient (based upon frontal area) increases 50 percent because of the reduction in T_w/T_∞ from 2.59 to 1.5. As the method of reference 9 is a zero heat-transfer method, its application to the heat-transfer case may be considered only qualitatively correct. It is reasonable to expect that the lack of any effect of heat transfer on the drag due to step roughness in the present investigation will not apply to smaller size roughness and that further investigation will be required for those conditions. In order to test the smaller step heights, an improved experimental technique is required to measure successfully the very small forces that will be encountered.

In the case of the wave roughness, the effect of smaller roughness height on the variation of $\Delta C_{D,s}$ with T_w/T_∞ should probably be considerably less severe because of the apparent nature of the flow differences. For the wave-type roughness, the nature of the boundary-layer effect might be expected to be that of cushioning the roughness with

a layer of slow moving air flowing over its surface in a gentle manner. The front face of the step roughness on the other hand is exposed to the full force of the oncoming boundary-layer flow which tends to impact with it. In this case, the forces contributed would be expected to be more sensitive to heat-transfer-produced changes in the boundary-layer profile than would those for the wave-type roughness.

Zero-heat-transfer data.- The zero-heat-transfer portion of the results of this investigation can be compared with similar existing results on the basis of h/δ, the ratio of roughness height to thickness of the boundary layer, as suggested in reference 4. The basis for this comparison is that similarity of flows will exist over two roughness elements when two roughnesses have the same shape, equal local Mach numbers, similar velocity profiles, and equal ratios of roughness height to boundary-layer thickness. The following simplifying assumptions are made in the present analysis. The quantity δ is estimated at the middle roughness position by means of the flat-plate approximation $\delta = \frac{\delta}{\theta}\theta$. The quantity δ/θ is from Tucker (ref. 10), and θ at the position of the middle roughness element is estimated by $\theta = \frac{x}{2} C_F$ where the skin friction is predicted by the method of Sommer and Short. (See ref. 7.) The quantity δ/θ from Tucker is chosen arbitrarily to correspond to a one-ninth-power velocity profile.

Steps with grooves: The results for the steps-with-grooves configuration are converted to roughness drag coefficient $C_{D,R}$ and presented on the basis of h/δ in figure 10. The data agree fairly well with the prediction of the method of reference 9 which is based on a quantity called "effective dynamic pressure." The predictions indicate that the effect of R_x on the drag coefficient is very large for a constant value of h/δ. This effect is due to the higher effective dynamic pressure that results from the changes in velocity profile with increase in R_x.

A more useful form for correlation of the step-roughness drag is suggested by the fact that a condition of constant h/δ and constant R_x corresponds to a constant R_h. The present data are shown in terms of R_h and R_x in figure 11. Included are the predictions based on reference 9 and experimental results from references 1 and 9. (For the experimental data the free-stream unit Reynolds number and axial distance to the middle of the series of roughness elements are used.) In this form it is easier to see the effect of variations in the independent variables x, h, and unit Reynolds number. The predicted values for the experimental conditions are indicated by the dashed lines which represent constant roughness height and varying unit Reynolds number. They indicate values generally 0 to 25 percent higher than the experimental values, except for the small steps at $M = 2.87$. This particular set of data is relatively inaccurate compared with the other data because of the low forces being measured.

It is interesting to note that the predictions slightly overestimated even the $M = 2.98$ data which were used in the group of data on which the correlation method is

based in reference 9. It can be seen from figure 11 that the prediction method of reference 9 is confirmed at $M = 3$ over a range of R_h from about 2000 to 60 000 (corresponding to step heights of 0.030 centimeter to 0.915 centimeter at a typical flight unit Reynolds number per meter of 6.5×10^6). The adequacy of the predictions at step-height Reynolds numbers outside of this range should be checked experimentally.

Wave roughness: The circular-arc wave data are presented in figure 12 and the sine-wave roughness results of reference 1 are shown for comparison. The drag coefficient appears to be approximately proportional to h/δ. The drag level decreases with increase in Mach number as might be expected from inviscid theory alone. But because the roughness shapes are not similar, a comparison in terms of the inviscid wave drag would be helpful.

The data can be compared more readily on the basis of an inviscid drag correlation parameter. The drag of a sine-wave surface can be shown to be $C_{D,R} = \frac{\pi^2}{\beta}\frac{h}{l}$ according to linearized two-dimensional theory, where $C_{D,R}$ is based on frontal area of the wave. Solving for the drag correlation parameter yields

$$\left(\frac{\beta}{h/l}\right)C_{D,R} = \pi^2 = 9.88$$

The data are presented in this form in figure 13. Included are pressure test results on sine-wave surfaces from McClure (ref. 11) and Anderson (ref. 12). The theoretical drag parameter values for the sine wave and circular-arc wave are shown for comparison. The present results compare reasonably well with the sine wave of reference 12 for which the average values of results for three waves (fourth, seventh, and eleventh) are shown. The results from reference 1 at $M = 1.6$ and 2.0 are brought into agreement, for both thickness ratios, and the effect of increasing h/l is to decrease the drag parameter $\frac{\beta C_{D,R}}{h/l}$. The result for the $h/l = 0.040$ $(M = 1.405)$ wave of reference 11 is at a condition where the flow effects are strongly nonlinear and for which linearized theory predicts too high a drag coefficient. It is probably for this reason that the data for this point fall so far from general correlation with data at other values of h/l.

The ratio h/δ can be divided by h/l to yield a parameter $\frac{h/\delta}{h/l} = l/\delta$ which is used in figure 14 as the variable. This form results in a correlation which is independent of thickness ratio for the lower range of h/l. At the higher values of h/l, the drag parameter decreased; thus a strong effect of thickness ratio appears to be present in this method of correlation.

Although the method presented for the correlation of the roughness drag of wave-shaped surfaces appears to do reasonably well, a wider range of data is required to prove

its generality. It would also be desirable to obtain results for values of h/δ both larger and smaller than are presently available.

CONCLUSIONS

An investigation has been conducted at a Mach number of 3 between unit Reynolds numbers per meter of 12×10^6 and 63×10^6 to determine the effect of heat transfer on the drag due to roughness of a steps-with-grooves configuration and a circular-arc-wave configuration in a turbulent boundary layer by means of force tests.

1. There was only a small effect of heat transfer on the roughness drag for either the wave or the step-with-grooves configuration at the conditions of this investigation, but this result may not be true for smaller values of step heights.

2. The zero-heat-transfer drag for both the wave and the steps with grooves were in good agreement with other experimental data.

3. The step-roughness drag coefficient data at Mach 3 were found to be correlated conveniently on the basis of two Reynolds numbers: one based upon roughness height, the other based on axial distance to the roughness.

4. It was found that a previously published roughness drag calculation method based upon "effective dynamic pressure" predicts available experimental data reasonably well at Mach 3 over a range of step-height roughness Reynolds numbers from about 2000 to 60 000.

5. For the wave-type roughness, an inviscid-type drag parameter $\frac{\beta C_{D,R}}{h/l}$ was found to vary with the ratio of roughness height to boundary-layer thickness h/δ as a unique function of roughness thickness ratio h/l. The drag parameter decreases with increase in thickness ratio.

6. At the lower values of thickness ratio, the drag parameter for the wave-type roughness results is related only to the ratio of the cycle length to the boundary-layer thickness.

Langley Research Center,
National Aeronautics and Space Administration,
Langley Station, Hampton, Va., May 14, 1968,
126-13-02-11-23.

APPENDIX

MACH NUMBER CALIBRATION

Because the reliability of experimental skin-friction data depended on an accurate assessment of test-section Mach number, several calibration tests were conducted as part of the present investigation. Two survey devices were used for obtaining pressure data required in computing Mach number. One was a vertically mounted survey rake which extended through the test section and measured static pressure, total pressure behind a normal shock, and stagnation temperature at 3, 8, and 12 vertical stations, respectively. A sketch of this rake is shown in figure 15(a). The other survey device was a center-line pitot-static probe and was sting mounted. This probe, shown in figure 15(b), was a cone-cylinder configuration with a total-pressure orifice at the tip and four static-pressure orifices equally spaced circumferentially at each of three stations along the cylindrical afterbody. The vertical survey rake was used in three of the calibration tests, whereas the pitot-static center-line probe was used in two tests.

As in the skin-friction model tests, the survey tests were conducted at stagnation pressures of 414, 690, 1034, and 1380 kN/m^2 in ascending order and at stagnation temperatures of 422° K and 588° K. One test at 422° K using the vertical survey rake was conducted by varying the tunnel stagnation pressure in descending order from 1380 kN/m^2.

Pressures measured with the vertical survey rake and with the center-line pitot-static probe were used in computing Mach number from the following pressure ratios:

(a) Static pressure to tunnel stagnation pressure,

(b) Static pressure to total pressure behind a normal shock, and

(c) Total pressure behind a normal shock to tunnel stagnation pressure.

Mach number was also computed from the ratio of static pressure to tunnel stagnation pressure by using pressures measured from test-section-wall static-pressure orifices.

Results obtained from the tests are summarized in figure 16. The variation of Mach number with tunnel stagnation pressure at stagnation temperatures of 422° K and 588° K is shown. The present results show a random variation of Mach number with tunnel stagnation conditions. This variation is thought to be a consequence of heat-transfer effects on nozzle geometry and boundary-layer growth.

When these results were applied to the skin-friction drag tests, consideration was given to the various methods of computation shown in figure 16, and it was concluded that a specific value of Mach number for each stagnation pressure level could not be established. Instead, an average Mach number of 2.977 was judged to be representative over the entire stagnation pressure range of the investigation and accurate to within 1/2 percent or ±0.015.

REFERENCES

1. Czarnecki, K. R.; Sevier, John R., Jr.; and Carmel, Melvin M.: Effects of Fabrication-Type Roughness on Turbulent Skin Friction at Supersonic Speeds. NACA TN 4299, 1958.

2. Czarnecki, K. R.; and Monta, William J.: Pressure Distributions Due to Two-Dimensional Fabrication-Type Surface Roughness on an Ogive Cylinder at Mach Numbers of 1.61 and 2.01. NASA TN D-835, 1961.

3. Czarnecki, K. R.; and Monta, William J.: Pressure Distributions Due to Fabrication-Type Roughness on an Ogive Cylinder at Transonic Speeds. NASA TN D-3516, 1966.

4. Czarnecki, K. R.; and Monta, William J.: Pressure Drags Due to Two-Dimensional Fabrication-Type Surface Roughness on an Ogive Cylinder at Transonic Speeds. NASA TN D-3519, 1966.

5. Czarnecki, K. R.; Jackson, Mary W.; and Monta, William J.: Studies of Skin Friction at Supersonic Speeds. NASA Conference on Supersonic-Transport Feasibility Studies and Supporting Research. NASA TM X-905, 1963, pp. 177-189.

6. Schaefer, William T., Jr.: Characteristics of Major Active Wind Tunnels at the Langley Research Center. NASA TM X-1130, 1965.

7. Sommer, Simon C.; and Short, Barbara J.: Free-Flight Measurements of Turbulent-Boundary-Layer Skin Friction in the Presence of Severe Aerodynamic Heating at Mach Numbers From 2.8 to 7.0. NACA TN 3391, 1955.

8. Peterson, John B., Jr.; and Monta, William J.: Considerations Regarding the Evaluation and Reduction of Supersonic Skin Friction. NASA TN D-3588, 1966.

9. Aircraft Div., Douglas Aircraft Co., Inc.: Investigation of Skin-Friction Drag on Practical Construction Surfaces for the Supersonic Transport. FDL TDL 64-74, U.S. Air Force, Aug. 1964.

10. Tucker, Maurice: Approximate Calculation of Turbulent Boundary-Layer Development in Compressible Flow. NACA TN 2337, 1951.

11. McClure, James Doyle: On Perturbed Boundary Layer Flows. Fluid Dyn. Res. Lab. Rep. No. 62-2 (Grant AF-AFOSR-62-187), Massachusetts Inst. Technol., June 1962.

12. Anderson, William J.: Supersonic Wind Tunnel Tests of Wavy-Walled Cylinders. ARL 65-203, U.S. Air Force, Oct. 1965. (Available from DDC as AD626932.)

TABLE I.- ORIFICE LOCATIONS

Orifice	x, cm	ϕ, deg
1	3.88	0
2	10.29	0
3	18.52	0
4	28.04	0
5	28.04	90
6	28.04	180
7	28.04	270
8	33.12	0
9	38.20	0
10	43.28	0
11	48.36	0
12	53.44	0
13	58.52	0
14	63.60	0
15	68.68	0
16	71.22	0
17	73.76	0
18	76.30	0
19	78.84	0

TABLE II.- THERMOCOUPLE LOCATIONS

Thermocouple	x, cm at $\phi = 270^{o}$
1	12.7
2	31.8
3	50.8
4 and A*	69.9
5 and B*	88.9
6	108.0
7	221.0
8	240.0
9	259.1
10	278.1
11 and C*	297.2

*Denotes thermocouples located at exterior surface.

TABLE III.- TEST PROGRAM

Run	Configuration	$p_{t,\infty}$, kN/m^2	$T_{t,\infty}$, ^oK	T_{model} at start of run
1	Smooth	414, 690, 1034 and 1380	422	T_{room}
2	Smooth	414, 690, 1034 and 1380	422	T_{room}
3	Smooth	414, 690, 1034 and 1380	588	T_{room}
4	Smooth	1380	422	T_{room}
5	Smooth	414, 690, 1034 and 1380	588	T_{room}
6	Smooth	414, 690, 1034 and 1380	422	T_{room}
7	Smooth	414, 690, 1034 and 1380	422	T_{room}
8	Smooth	414, 690, 1034 and 1380	422	T_{aw}
9	0.104-cm steps with grooves	414, 690, 1034 and 1380	422	T_{room}
10	0.104-cm steps with grooves	414, 690, 1034 and 1380	588	T_{room}
11	0.104-cm steps with grooves	414, 690, 1034 and 1380	422	T_{aw}
12	0.302-cm circular-arc waves	414, 690, 1034 and 1380	422	T_{room}
13	0.302-cm circular-arc waves	414, 690, 1034 and 1380	588	T_{room}
14	0.302-cm circular-arc waves	414, 690, 1034 and 1380	422	T_{aw}

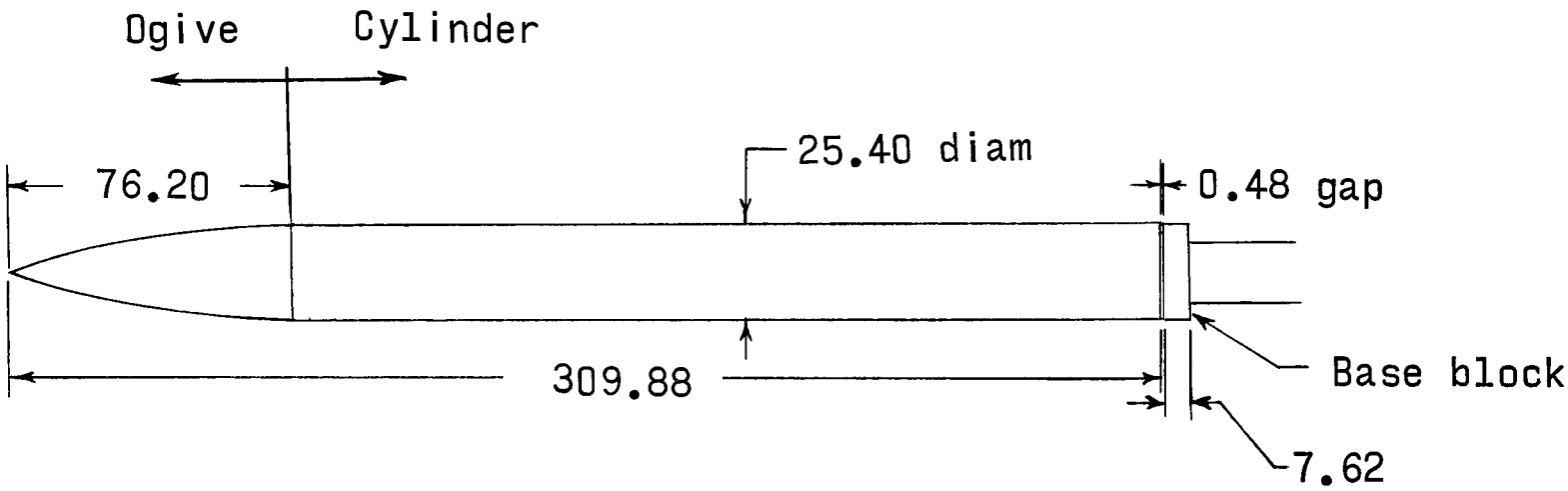

(a) Basic body.

Figure 1.- Sketch of model. (All dimensions are in centimeters except as noted.)

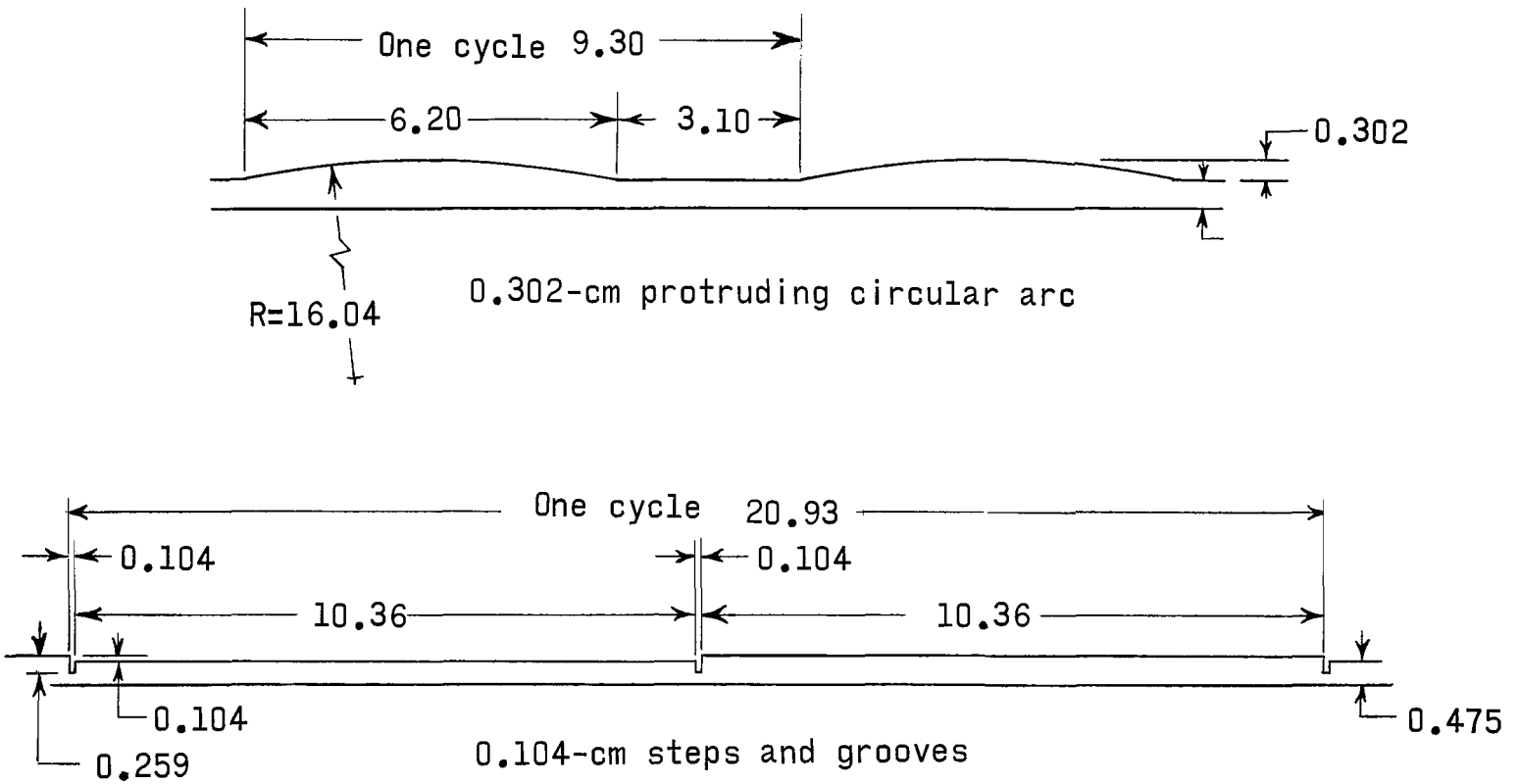

(b) Roughness configurations.

Figure 1.- Concluded.

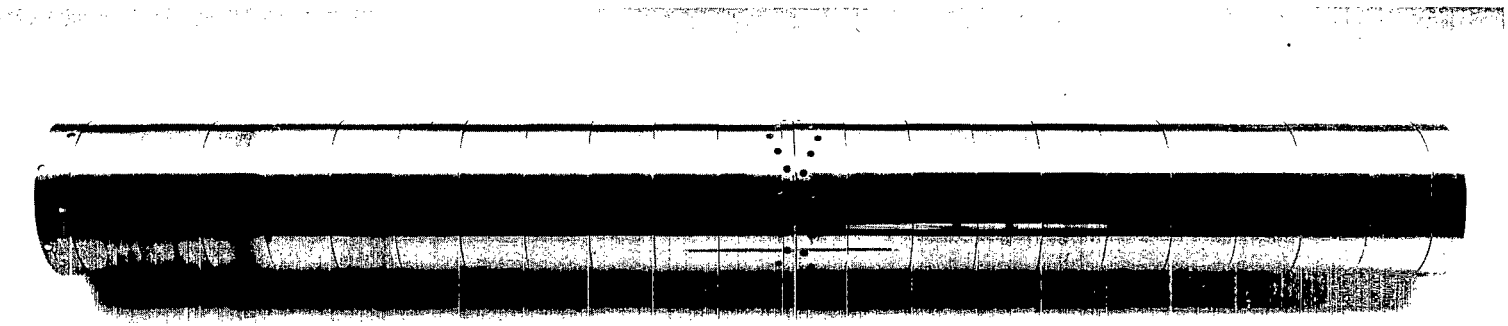

(a) 0.104-cm steps with grooves.

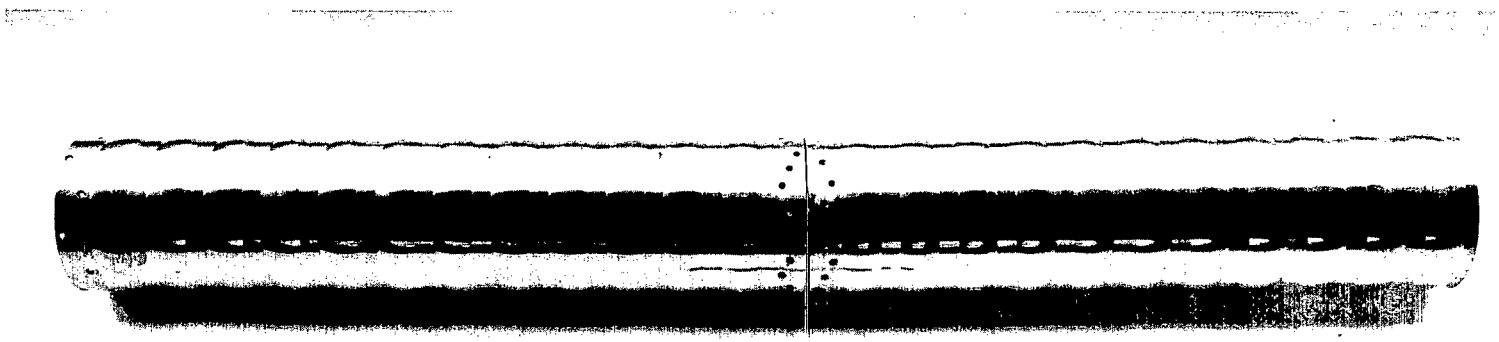

(b) 0.302-cm protruding arc waves. L-68-896

Figure 2.- Photographs of cylindrical model sections that contain fabrication-type roughness.

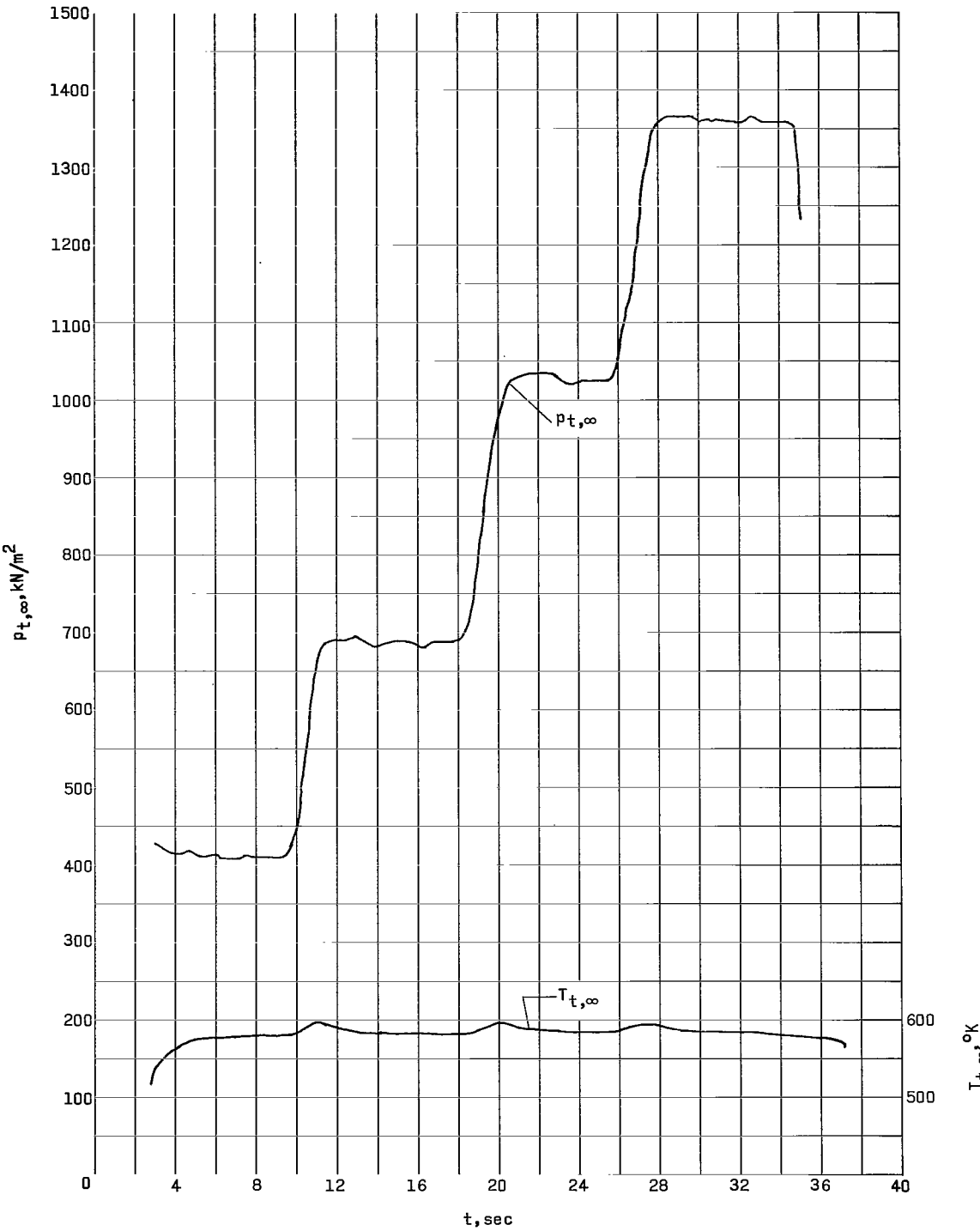

Figure 3.- Typical variation of tunnel stagnation temperature and pressure with time. $T_{t,\infty} \approx 588^0$ K.

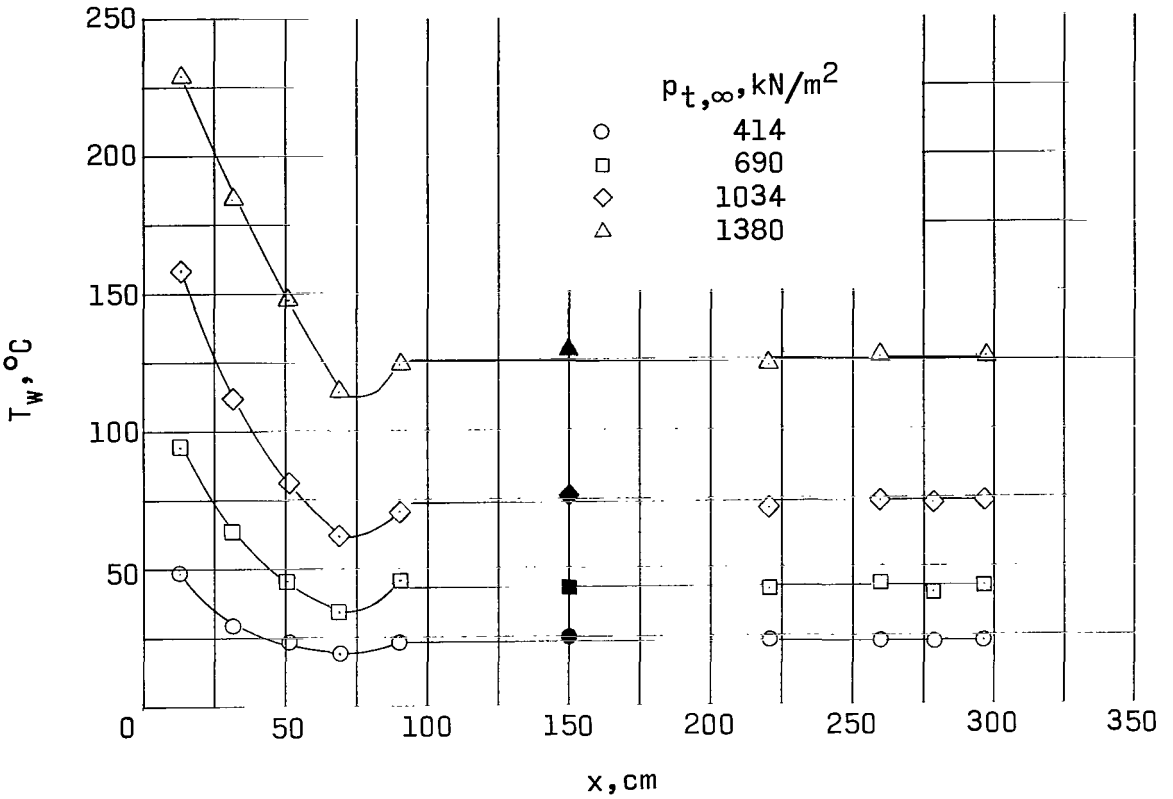

(a) $T_{t,\infty} \approx 588^0$ K.

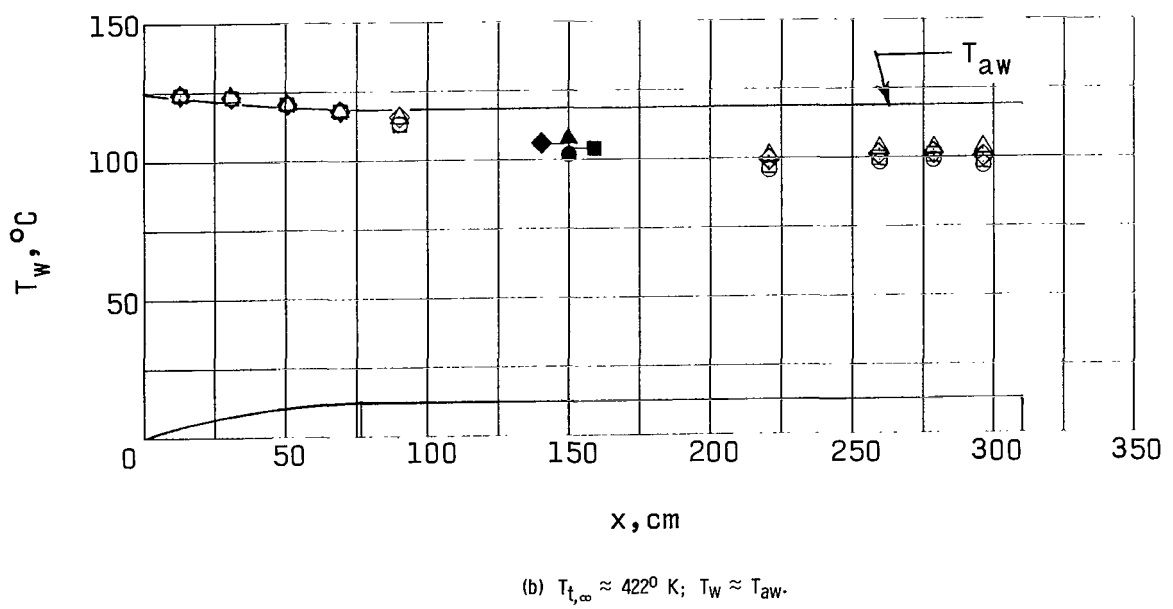

(b) $T_{t,\infty} \approx 422^0$ K; $T_w \approx T_{aw}$.

Figure 4.- Typical axial temperature distributions for the smooth ogive cylinder. Solid symbols denote weighted-average model surface temperature.

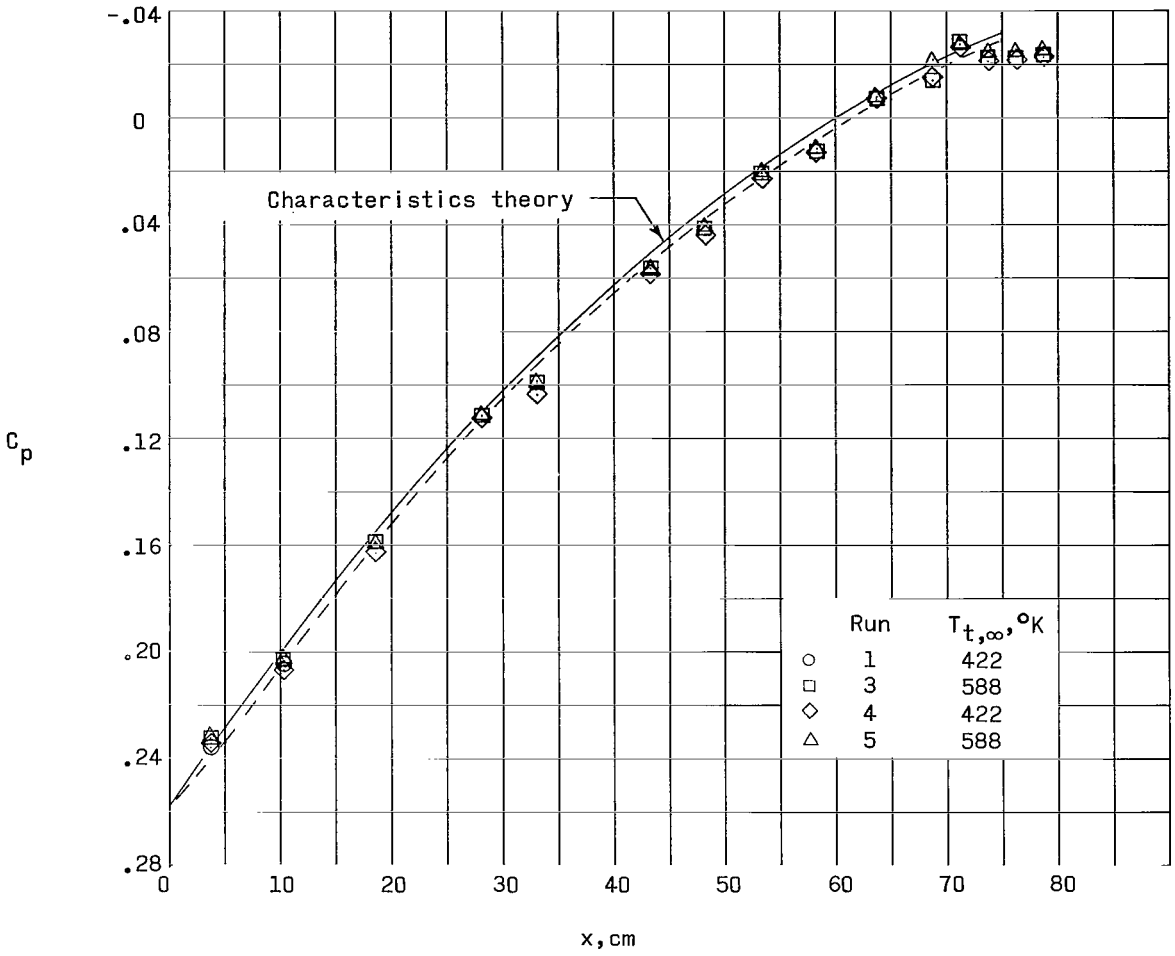

(a) Longitudinal distribution; $\Phi = 0^0$.

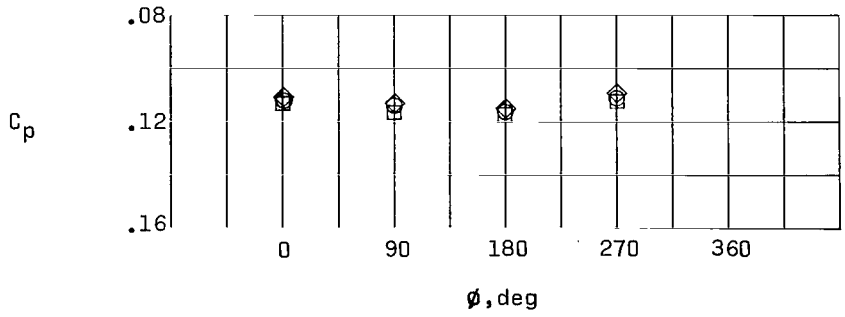

(b) Circumferential distribution; x = 28.04 cm.

Figure 5.- Experimental and theoretical pressure distributions for the ogive nose. $p_{t,\infty}$ = 1379 kN/m^2.

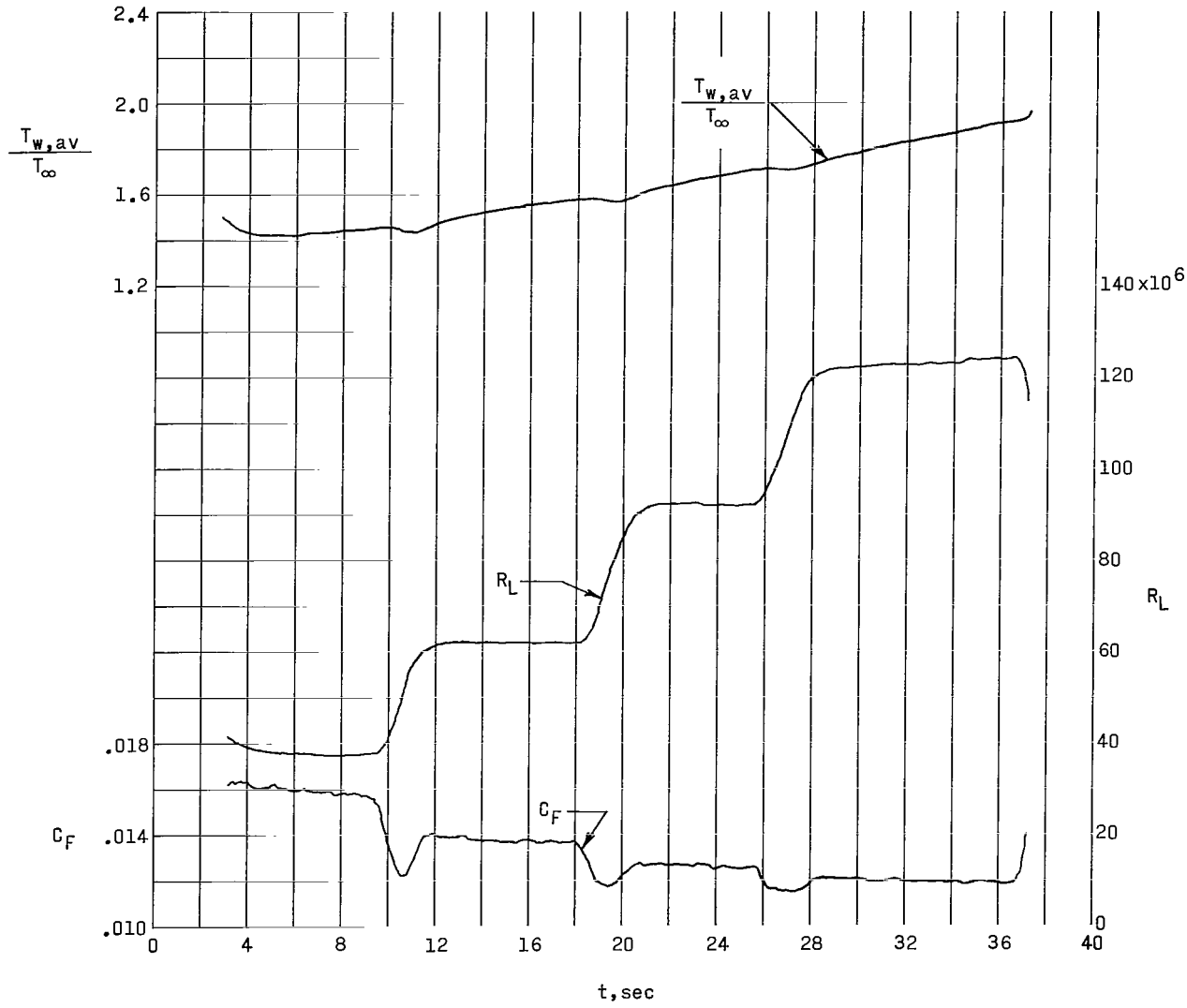

Figure 6.- Typical variations with time of ratio of wall temperature to free-stream temperature, Reynolds number, and average skin-friction drag coefficient. $T_{t,\infty} \approx 588^0$ K.

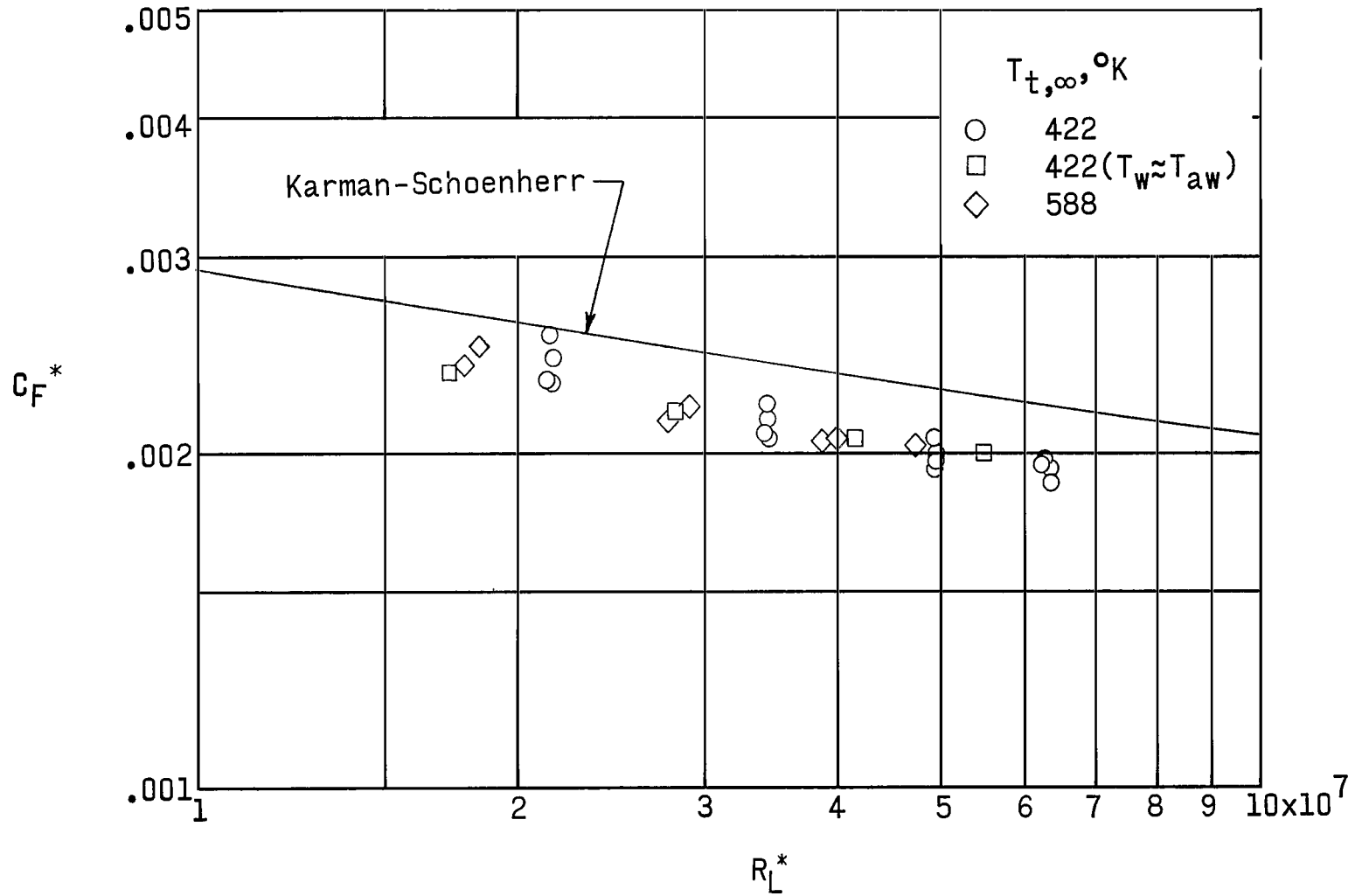

Figure 7.- Variation of experimental drag coefficient with Reynolds number in transformed plane.

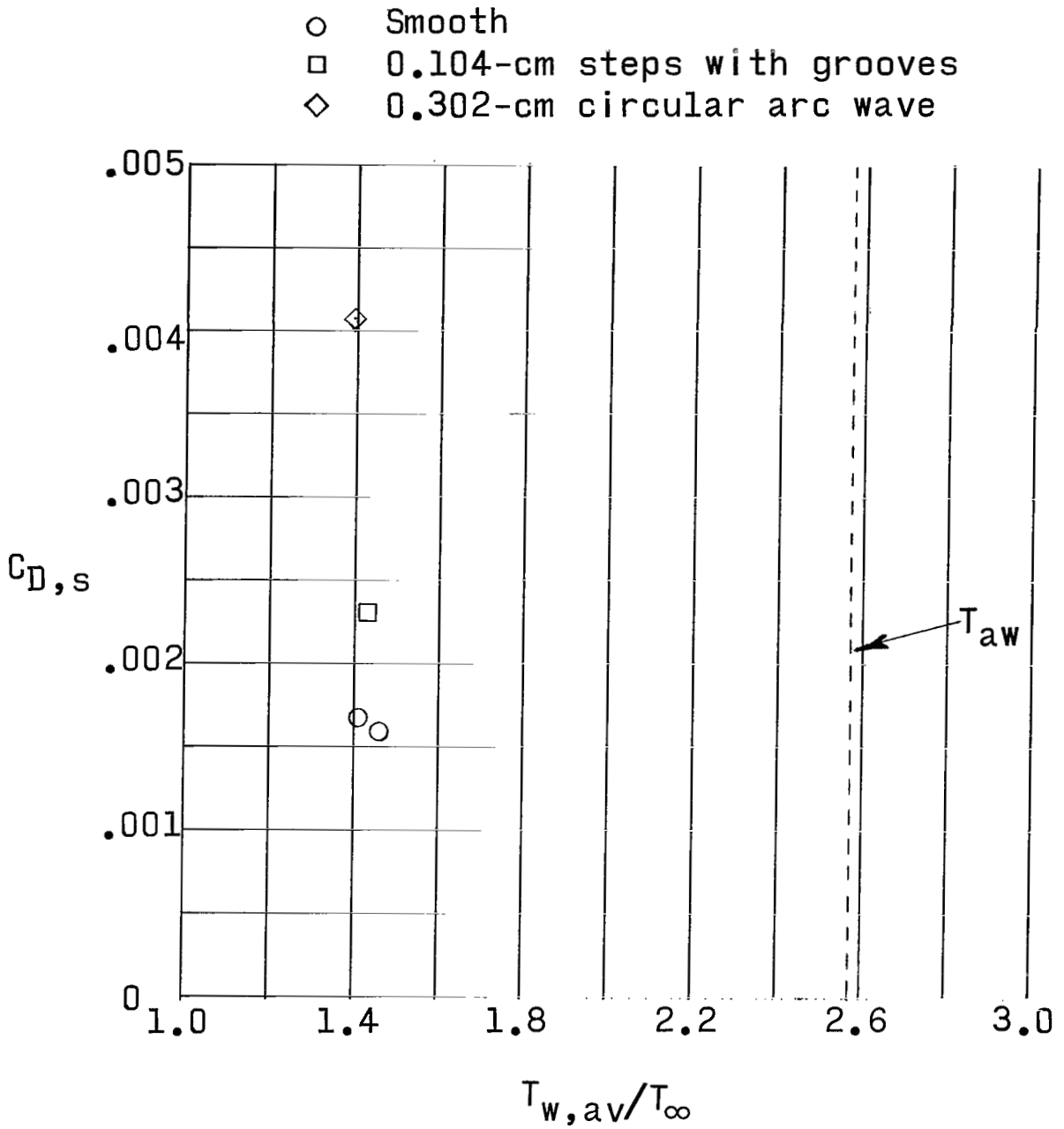

(a) $R_L \approx 37.8 \times 10^6$.

Figure 8.- Variation of surface-drag coefficient with wall temperature ratio for all models.

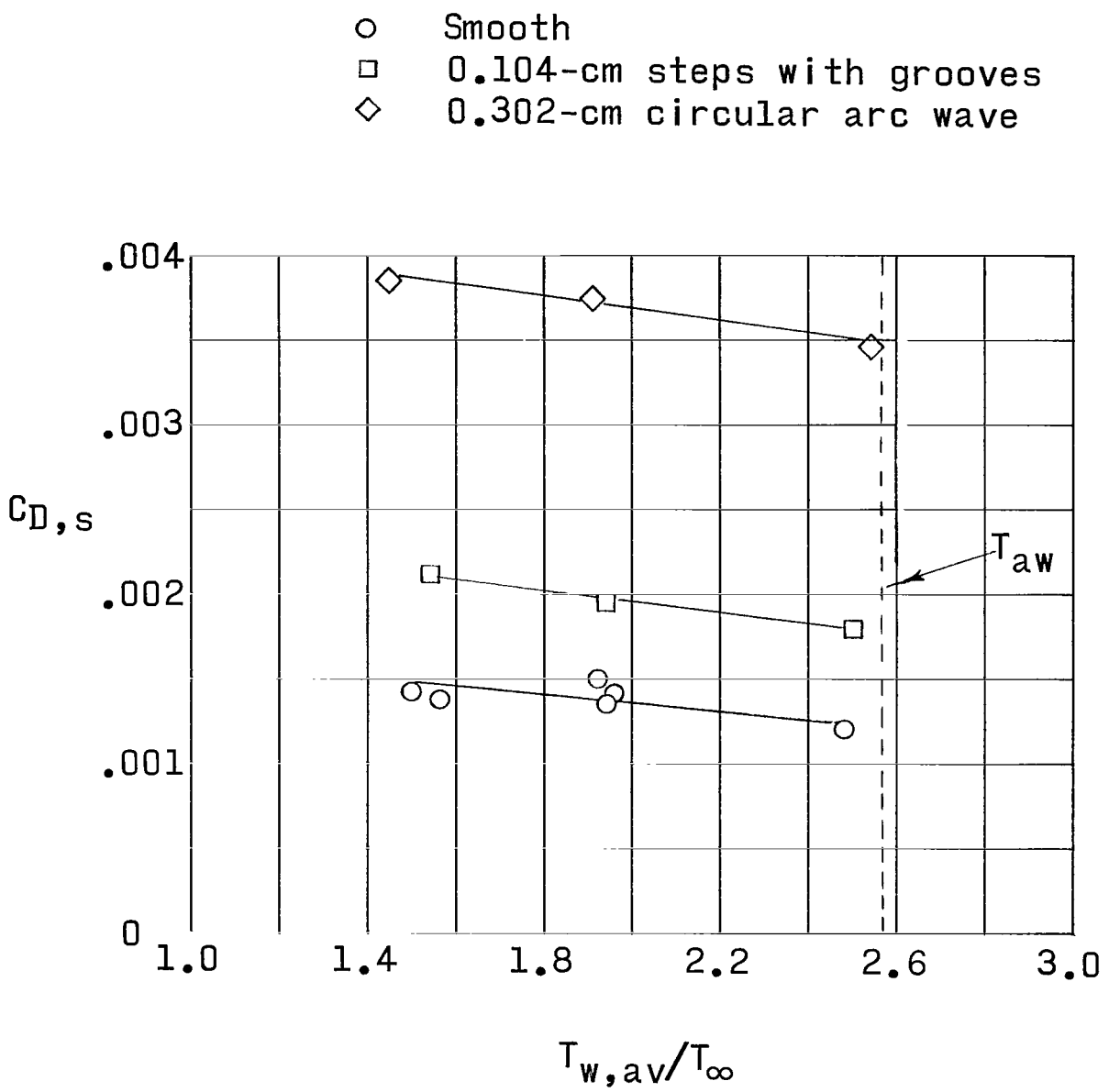

(b) $R_L \approx 59.4 \times 10^6$.

Figure 8.- Continued.

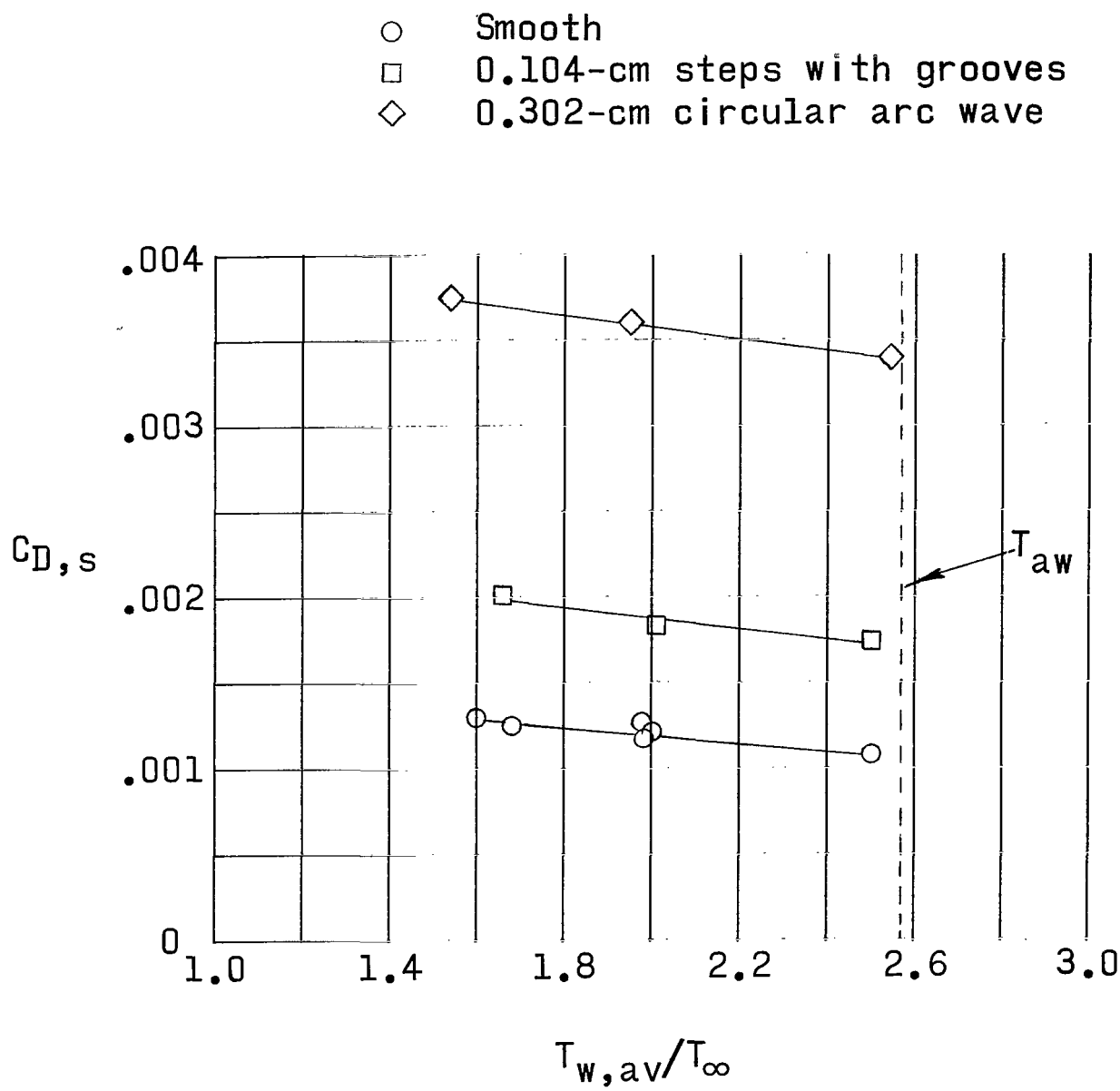

(c) $R_L \approx 95.6 \times 10^6$.

Figure 8.- Continued.

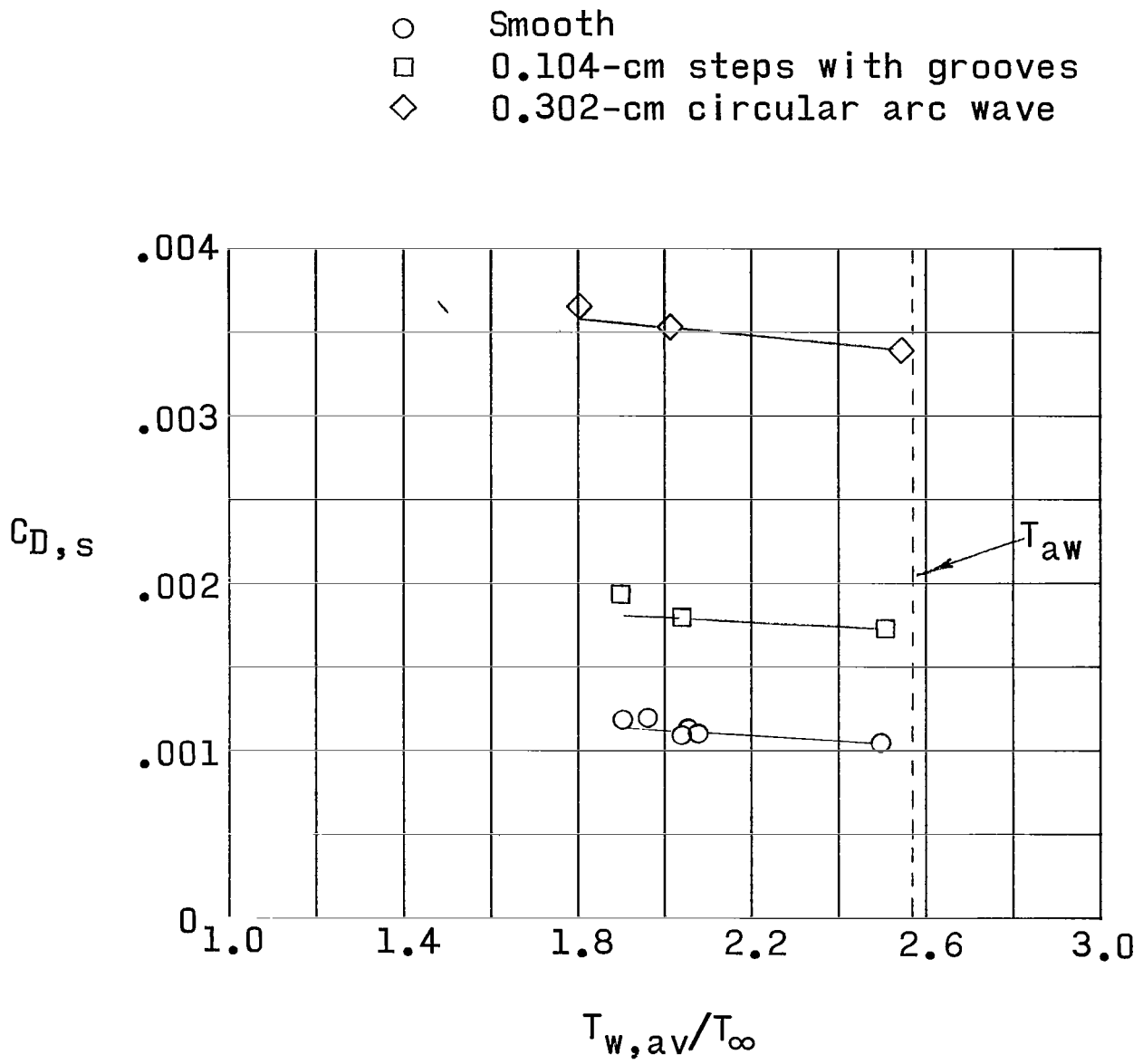

(d) $R_L \approx 145 \times 10^6$.

Figure 8.- Continued.

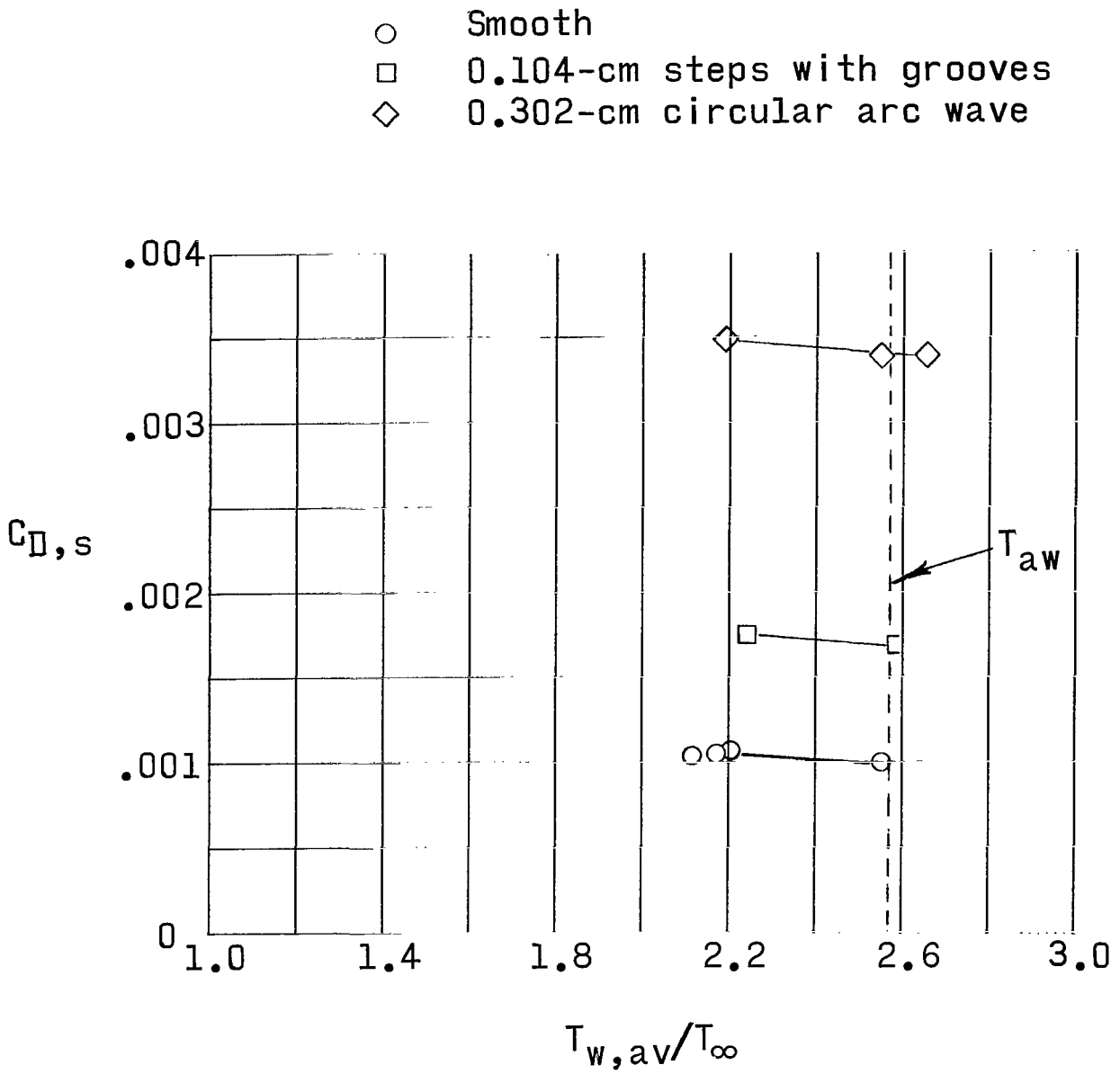

(e) $R_L \approx 196 \times 10^6$.

Figure 8.- Concluded.

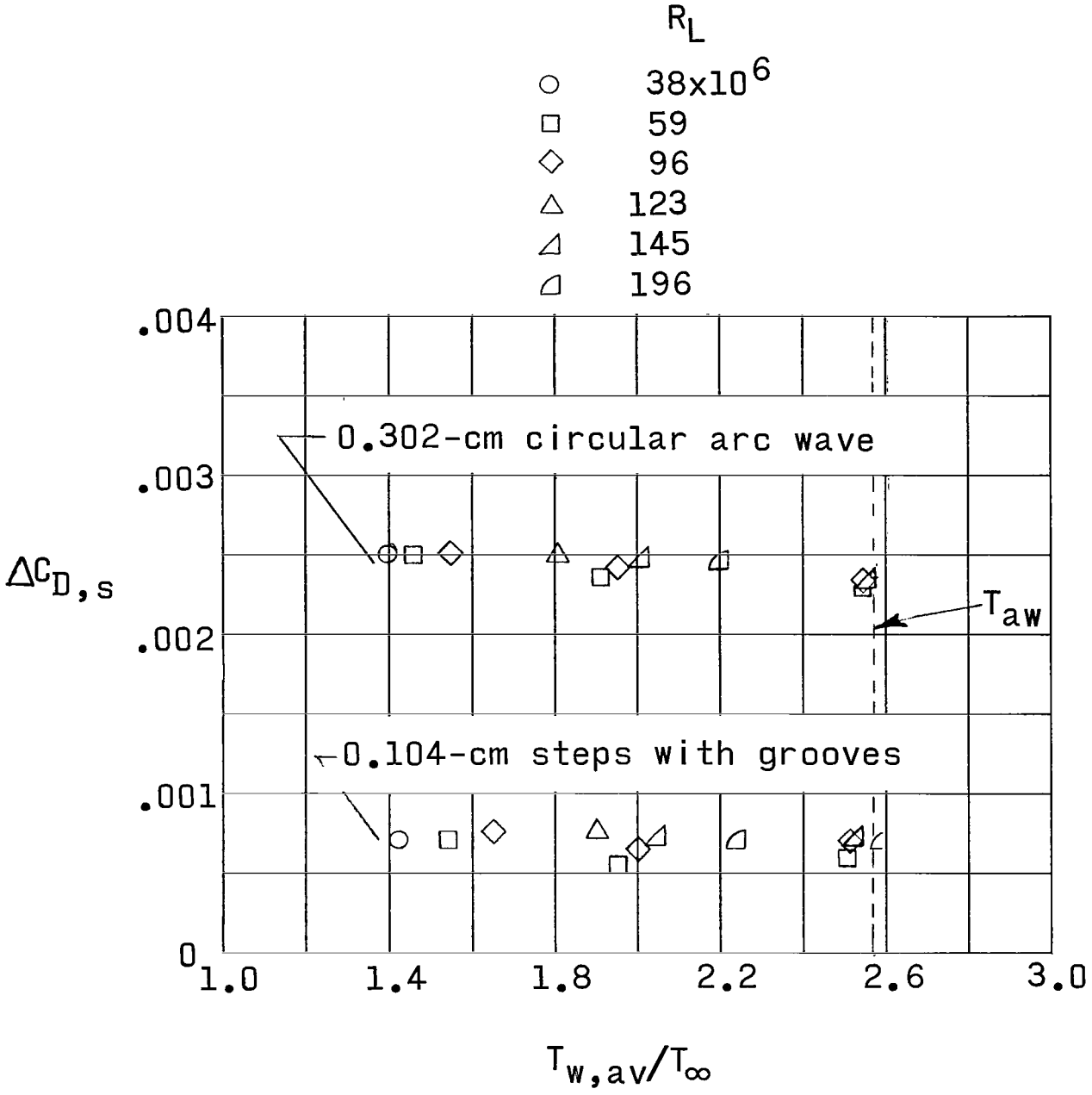

Figure 9.- Variation of incremental drag coefficient with wall temperature ratio.

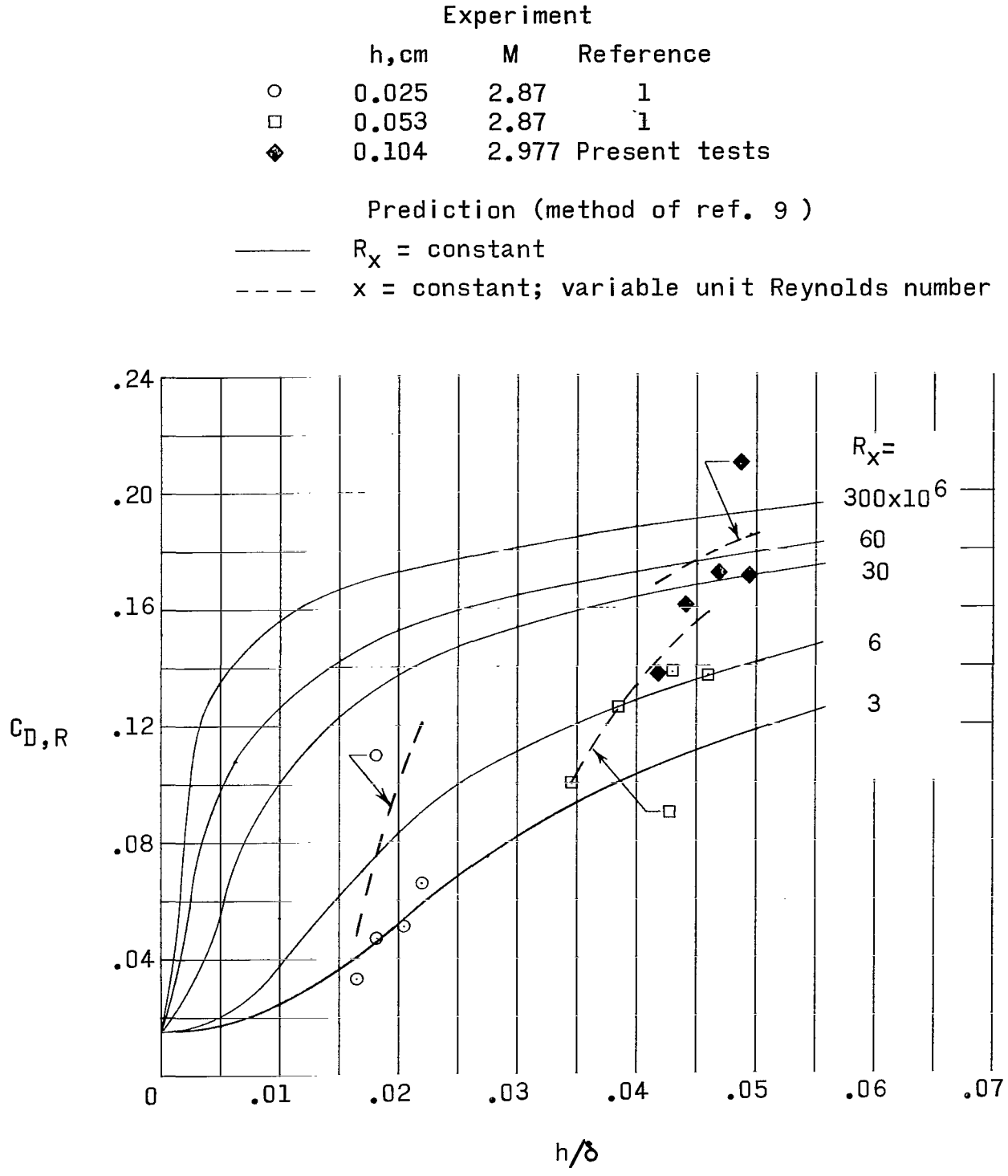

Figure 10.- Comparison of experimental and predicted variation of $C_{D,R}$ with h/δ for combination-step roughness. $T_w \approx T_{aw}$.

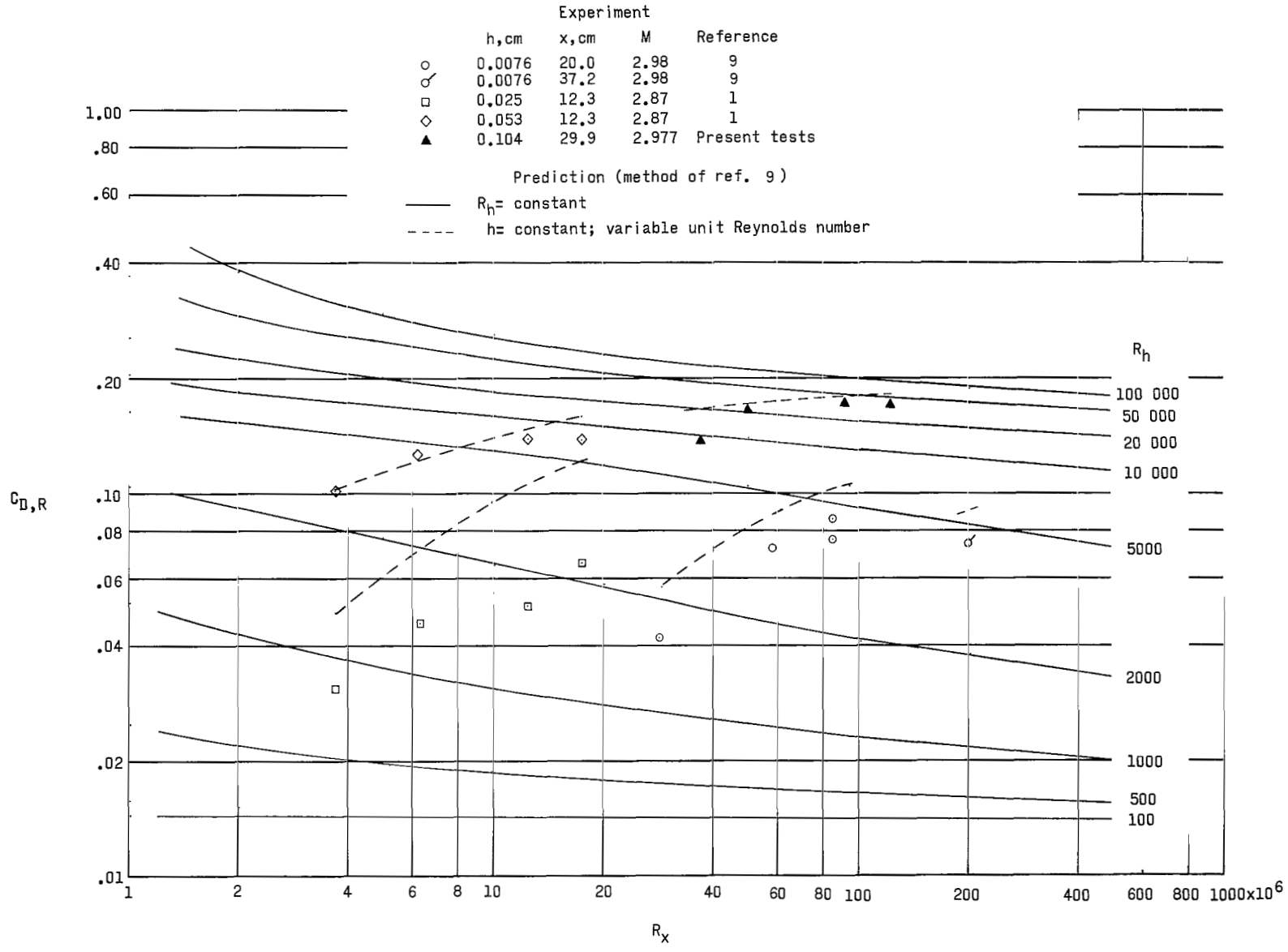

Figure 11.- Comparison of experimental and predicted variation of $C_{D,R}$ with R_x and R_h for combination-step roughness. $T_w \approx T_{aw}$.

	M	Configuration h, cm	l, cm	
⊙	1.61	0.061	3.81	sine wave (ref. 1)
○	1.61	.135	3.81	sine wave (ref. 1)
⊡	2.01	.061	3.81	sine wave (ref. 1)
□	2.01	.135	3.81	sine wave (ref. 1)
▲	2.98	.302	6.20	circular-arc wave (present tests)

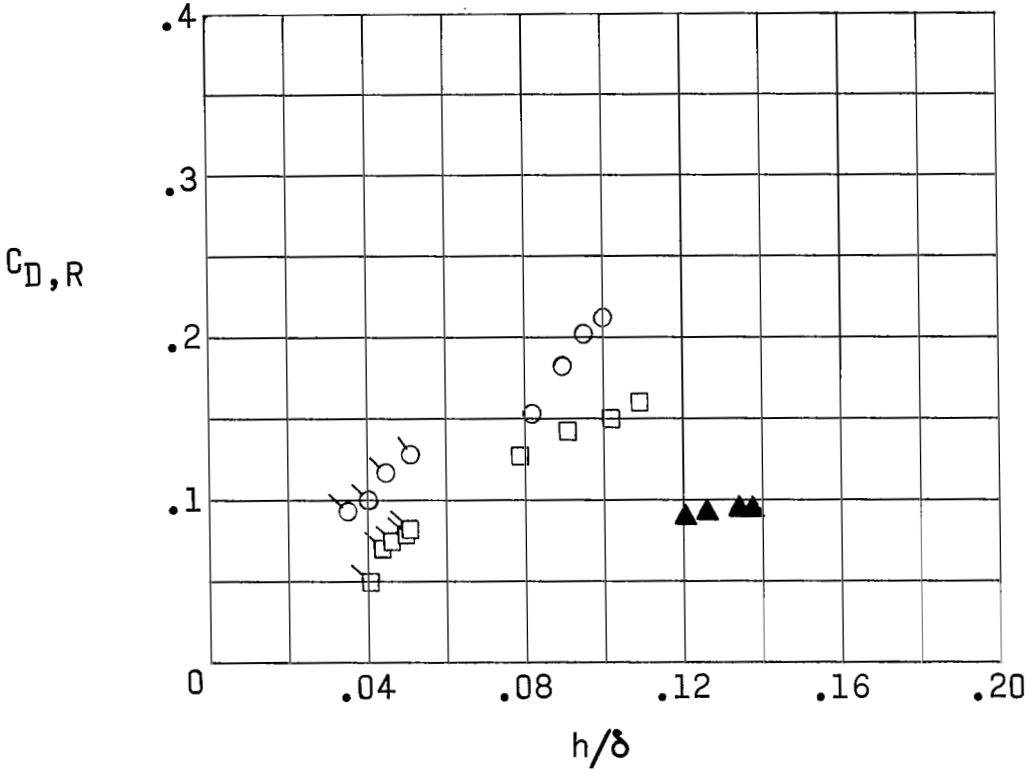

Figure 12.- Variation of roughness drag coefficient with the roughness height to boundary-layer-thickness ratio for wave roughness. $T_{w,av} \approx T_{aw}$.

——— Theory, $\delta = 0$

	M	h/l	h, cm	l, cm	Configuration
○ ⟋	1.61, 2.01	0.016	0.061	3.81	sine wave (ref. 1)
□	1.405	.020	.102	5.08	sine wave (ref. 11)
◇ ⟋	1.61, 2.01	.035	.135	3.81	sine wave (ref. 1)
△	1.405	.040	.203	5.08	sine wave (ref. 11)
◢	2.977	.049	.302	6.20	circular-arc wave (present tests)
◿	3.00	.051	.203	3.99	sine wave (ref. 12)

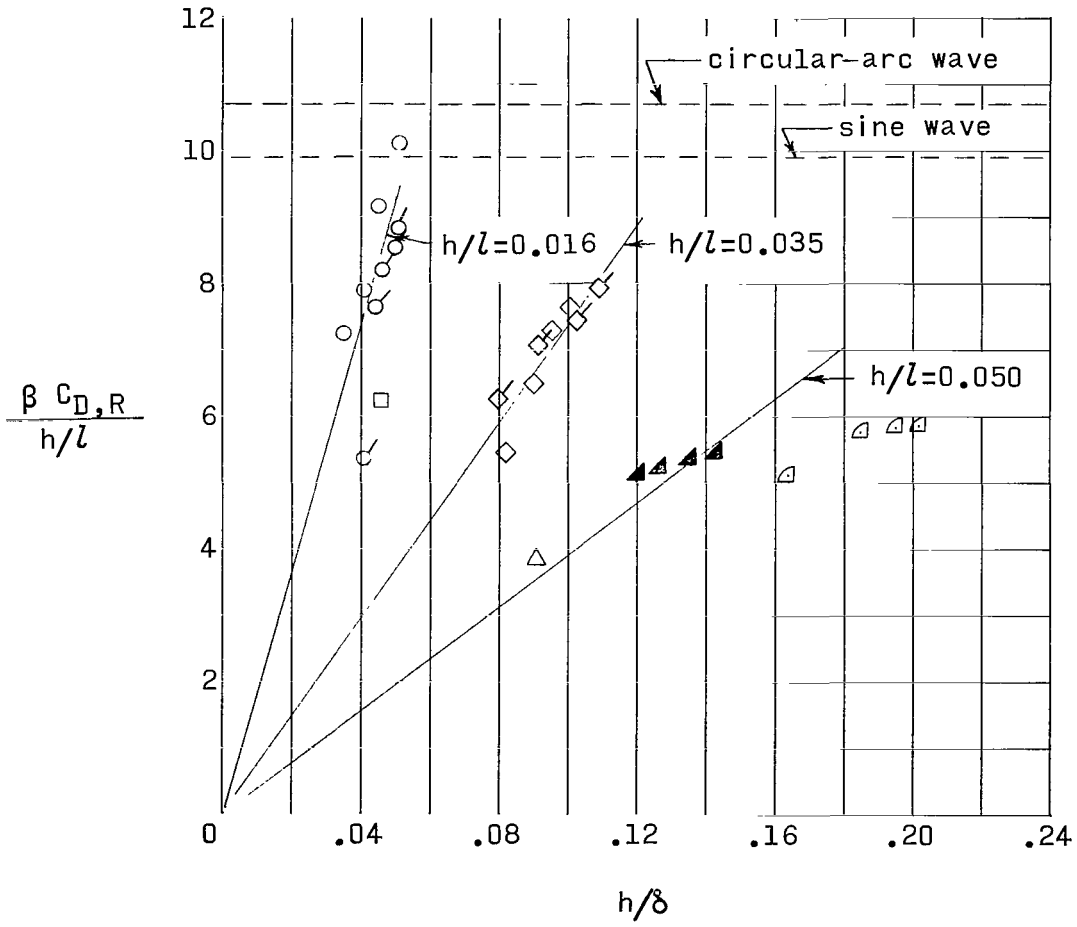

Figure 13.- Variation of drag parameter $\frac{\beta C_{D,R}}{h/l}$ with ratio of roughness height to boundary-layer thickness.

— — Theory, $\delta = 0$

	M	Configuration h/l	h, cm	l, cm	
○ ♂	1.61, 2.01	0.016	0.061	3.81	sine wave (ref. 1)
□	1.405	.020	.102	5.08	sine wave (ref. 11)
◇ ♂	1.61, 2.01	.035	.135	3.81	sine wave (ref. 1)
△	1.405	.040	.203	5.08	sine wave (ref. 11)
◢	2.977	.049	.302	6.20	circular-arc wave (present tests)
◿	3.00	.051	.203	3.99	sine wave (ref. 12)

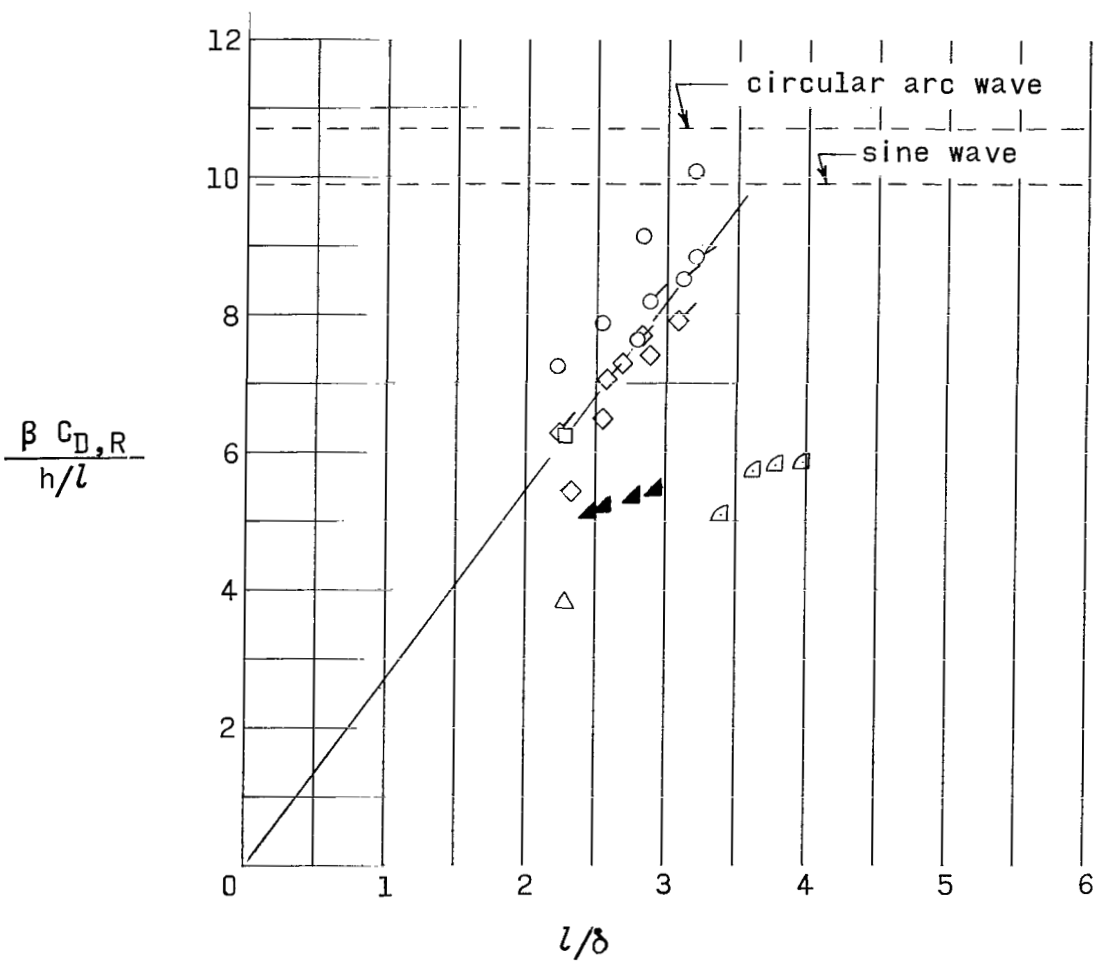

Figure 14.- Variation of drag parameter $\frac{\beta C_{D,R}}{h/l}$ with ratio of roughness length to boundary-layer thickness.

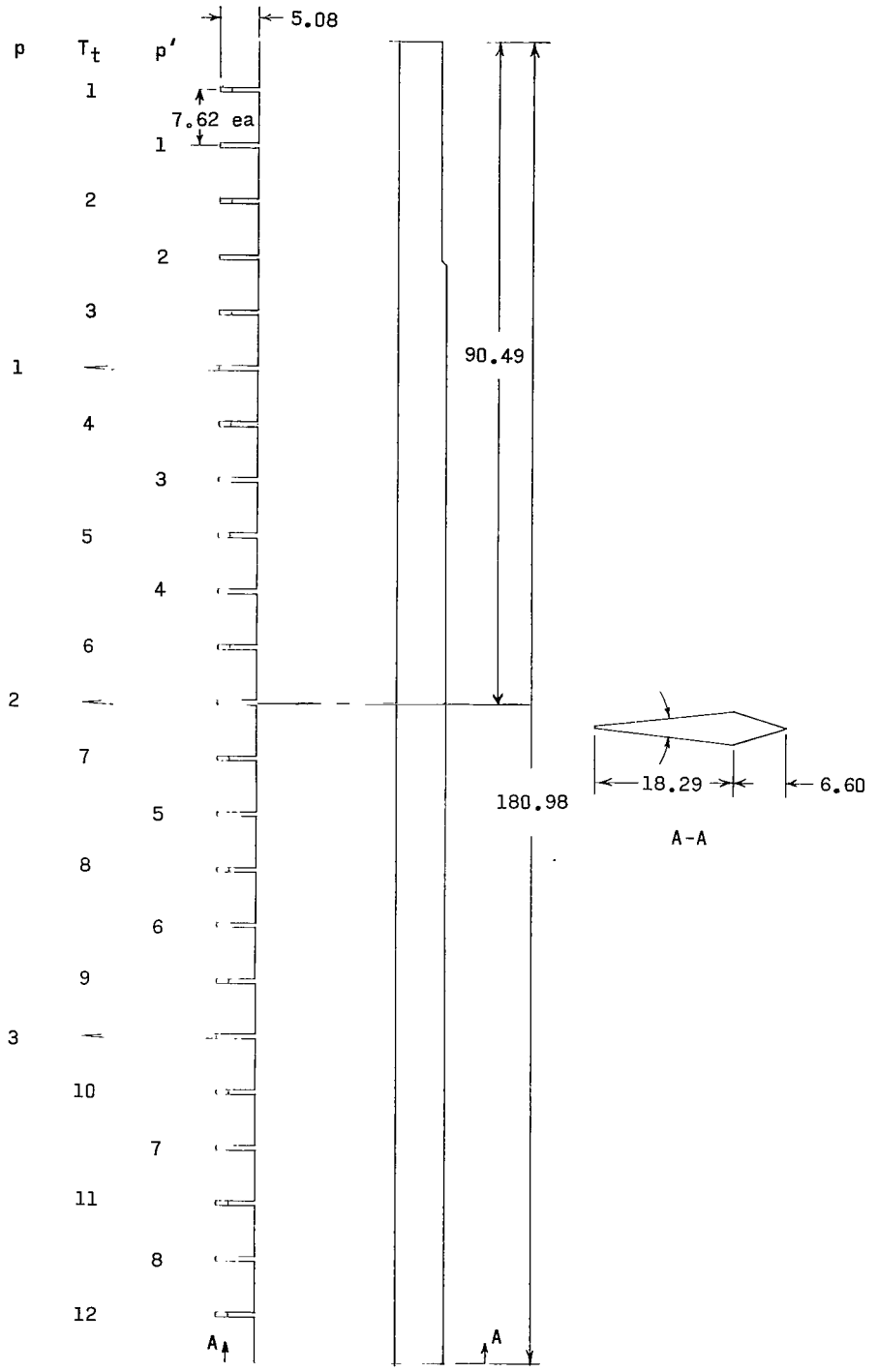

(a) Vertical survey rake.

Figure 15.- Sketch of wind-tunnel calibration devices. All dimensions are in centimeters except as noted.

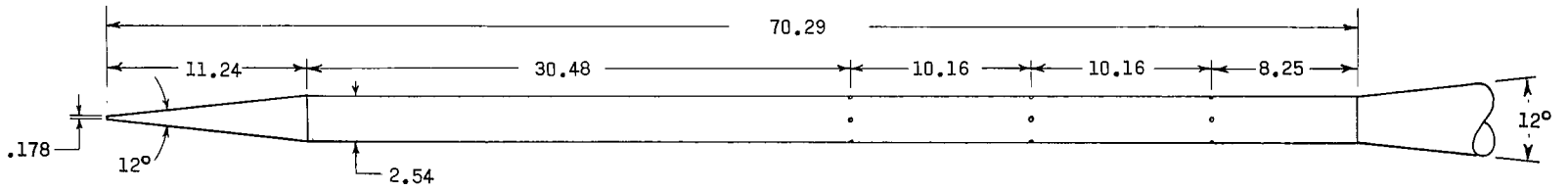

(b) Center-line pitot-static probe.

Figure 15.- Concluded.

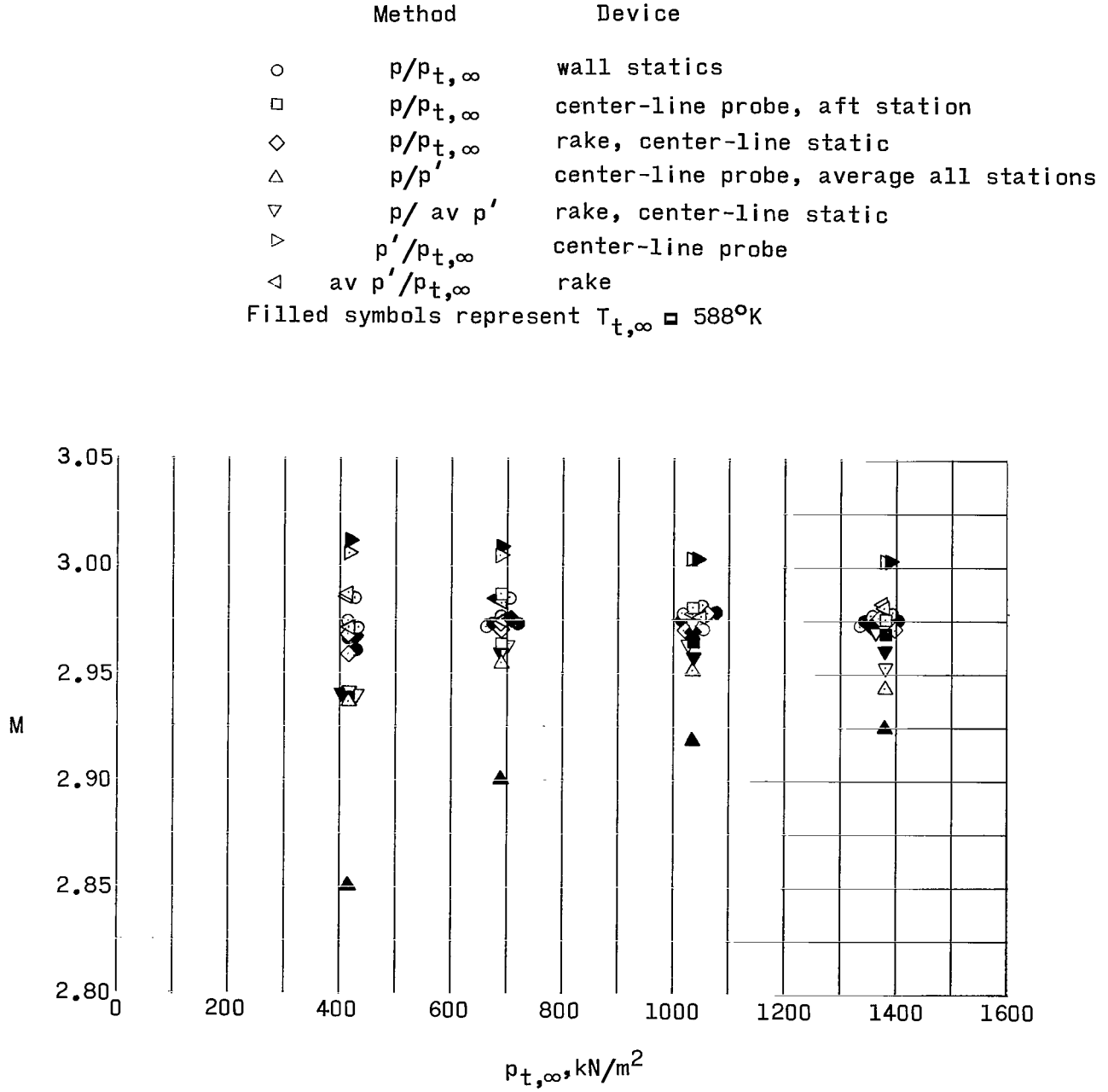

Figure 16.- Test-section Mach number as measured with two calibration devices. $T_{t,\infty}$ = 422° K and 588° K.

NATIONAL AERONAUTICS AND SPACE ADMINISTRATION
WASHINGTON, D. C. 20546

OFFICIAL BUSINESS

FIRST CLASS MAIL

POSTAGE AND FEES PAID
NATIONAL AERONAUTICS AND
SPACE ADMINISTRATION

POSTMASTER: If Undeliverable (Section 158 Postal Manual) Do Not Return

"The aeronautical and space activities of the United States shall be conducted so as to contribute . . . to the expansion of human knowledge of phenomena in the atmosphere and space. The Administration shall provide for the widest practicable and appropriate dissemination of information concerning its activities and the results thereof."

— NATIONAL AERONAUTICS AND SPACE ACT OF 1958

NASA SCIENTIFIC AND TECHNICAL PUBLICATIONS

TECHNICAL REPORTS: Scientific and technical information considered important, complete, and a lasting contribution to existing knowledge.

TECHNICAL NOTES: Information less broad in scope but nevertheless of importance as a contribution to existing knowledge.

TECHNICAL MEMORANDUMS: Information receiving limited distribution because of preliminary data, security classification, or other reasons.

CONTRACTOR REPORTS: Scientific and technical information generated under a NASA contract or grant and considered an important contribution to existing knowledge.

TECHNICAL TRANSLATIONS: Information published in a foreign language considered to merit NASA distribution in English.

SPECIAL PUBLICATIONS: Information derived from or of value to NASA activities. Publications include conference proceedings, monographs, data compilations, handbooks, sourcebooks, and special bibliographies.

TECHNOLOGY UTILIZATION PUBLICATIONS: Information on technology used by NASA that may be of particular interest in commercial and other non-aerospace applications. Publications include Tech Briefs, Technology Utilization Reports and Notes, and Technology Surveys.

Details on the availability of these publications may be obtained from:

SCIENTIFIC AND TECHNICAL INFORMATION DIVISION

NATIONAL AERONAUTICS AND SPACE ADMINISTRATION

Washington, D.C. 20546